Atmos. Chem. Phys., 10, 2825–2845, 2010
www.atmos-chem-phys.net/10/2825/2010/

Atmospheric Chemistry and Physics

Characterization of a large biogenic secondary organic aerosol event from eastern Canadian forests

J. G. Slowik[1], C. Stroud[2], J. W. Bottenheim[2], P. C. Brickell[2], R. Y.-W. Chang[1], J. Liggio[2], P. A. Makar[2], R. V. Martin[3,4], M. D. Moran[2], N. C. Shantz[1,2], S. J. Sjostedt[1], A. van Donkelaar[3], A. Vlasenko[1,2], H. A. Wiebe[2], A. G. Xia[2], J. Zhang[2], W. R. Leaitch[2], and J. P. D. Abbatt[1]

[1]University of Toronto, Department of Chemistry, Toronto, ON, Canada
[2]Environment Canada, Science and Technology Branch, Toronto, ON, Canada
[3]Dalhousie University, Department of Physics and Atmospheric Science, Halifax, NS, Canada
[4]Harvard-Smithsonian Center for Astrophysics, Atomic and Molecular Physics Division, Cambridge, MA, USA

Received: 3 July 2009 – Published in Atmos. Chem. Phys. Discuss.: 1 September 2009
Revised: 4 March 2010 – Accepted: 14 March 2010 – Published: 26 March 2010

Abstract. Measurements of aerosol composition, volatile organic compounds, and CO are used to determine biogenic secondary organic aerosol (SOA) concentrations at a rural site 70 km north of Toronto. These biogenic SOA levels are many times higher than past observations and occur during a period of increasing temperatures and outflow from Northern Ontario and Quebec forests in early summer. A regional chemical transport model approximately predicts the event timing and accurately predicts the aerosol loading, identifying the precursors as monoterpene emissions from the coniferous forest. The agreement between the measured and modeled biogenic aerosol concentrations contrasts with model underpredictions for polluted regions. Correlations of the oxygenated organic aerosol mass with tracers such as CO support a secondary aerosol source and distinguish biogenic, pollution, and biomass burning periods during the field campaign. Using the Master Chemical Mechanism, it is shown that the levels of CO observed during the biogenic event are consistent with a photochemical source arising from monoterpene oxidation. The biogenic aerosol mass correlates with satellite measurements of regional aerosol optical depth, indicating that the event extends across the eastern Canadian forest. This regional event correlates with increased temperatures, indicating that temperature-dependent forest emissions can significantly affect climate through enhanced direct optical scattering and higher cloud condensation nuclei numbers.

Correspondence to: J. P. D. Abbatt
(jabbatt@chem.utoronto.ca)

1 Introduction

There has been intense interest of late in the nature of the organic component of the tropospheric aerosol, specifically its complex composition, oxidation state, hygroscopicity, and reactivity. While a number of secondary organic aerosol (SOA) formation routes have been presented, there remain considerable uncertainties in determining the most significant pathways by which organic mass accumulates on tropospheric particles (Kanakidou et al., 2005; Goldstein and Galbally, 2007; Hallquist et al., 2009). The conventional perspective has been that reactive volatile organic compounds (VOCs) from biogenic emissions (e.g. monoterpenes and, more recently, isoprene) or anthropogenic sources (e.g. aromatic hydrocarbons) are oxidized to form less volatile products that then partition to particles. Comparisons of observed and modeled organic aerosol loadings have been examined in case studies of urban areas (Volkamer et al., 2006; Dzepina et al., 2009) and urban outflow, yielding a systematic underprediction by models that increases with photochemical age (Johnson et al., 2006; Volkamer et al., 2006; de Gouw et al., 2008). In contrast, biogenic aerosol studies in tropical (Claeys et al., 2004; Chen et al., 2009; Gunthe et al., 2009), subtropical (Kavouras et al., 1998; Capes et al., 2009), and boreal forests (Tunved et al., 2006) have mostly reported significantly lower concentrations than those observed over polluted regions, despite studies indicating that global VOC emissions are higher from biogenic sources (Guenther et al., 1996, 2000).

Published by Copernicus Publications on behalf of the European Geosciences Union.

However, some evidence exists that the biogenic SOA mass may be larger than previously observed. Higher biogenic SOA concentrations than those discussed above have been observed in a region of high terpene emissions (Shantz et al., 2004). Organic concentrations of 5.7 and 3.1 $\mu g/m^3$ were observed in eastern Canada during periods influenced by isoprene and monoterpene oxidation, respectively (Williams et al., 2007). However, the biogenic SOA mass fraction during these episodes is unknown. The interaction of biogenic VOCs with anthropogenic pollutants is hypothesized to contribute to high aerosol loadings in the southeast United States (Goldstein et al., 2009). Further, carbon isotope measurements suggest recent involvement in photosynthesis for the majority of organic aerosol carbon in a variety of settings, including polluted cases (Szidat et al., 2004; Weber et al., 2007). This finding makes comprehensive studies of biogenic aerosol formation events of extreme importance, to delineate the conditions under which biogenic aerosol readily forms and to describe the photochemical state of the atmosphere that is associated with such activity.

Here we present evidence for the formation of the most substantial biogenic organic aerosol formation event yet observed, from measurements at a rural location north of Toronto, Canada. The five day event is characterized by steadily increasing organic aerosol levels to a maximum of 15 μgm^{-3}, correlated strongly with increasing temperature. Atmospheric CO levels increase concurrently. Wind flow was from the largely unpopulated regions of northern and central Ontario and Quebec. Through both in situ observations and regional air quality modeling results, the organic aerosol is shown to be photochemically produced from biogenic precursors. The increasing levels of CO are consistent with a photochemical source as well. Satellite observations of aerosol optical depth (AOD) highlight the importance of these forested areas as major aerosol source regions that will affect climate, the regional ecology, and air quality.

2 Materials and methods

2.1 Sampling location

Sampling for the Egbert 2007 field campaign was conducted from 14 May to 15 June 2007, at the Center for Atmospheric Research Experiments (CARE) in Egbert, Ontario, Canada (44.23° N, 79.78° W; 251 m a.s.l). The Egbert CARE site is a permanent research station operated by Environment Canada. Egbert is a rural location consisting of mixed forest and farmland, approximately 70 km north of Toronto. Toronto is one of the largest urban areas in North America, with a population of 5 million, while the population of the Southern Ontario region is approximately 8 million. During periods of southerly winds, Egbert is influenced by the urban outflow of Toronto. In contrast, northerly winds bring air from sparsely populated, heavily forested regions. The only major anthropogenic sources to the north are from nickel and copper mining industries in the city of Sudbury (∼300 km to the north).

2.2 Instrumentation

2.2.1 Aerosol mass spectrometer

The size-resolved, non-refractory composition of submicron aerosol particles was measured with an Aerodyne time-of-flight aerosol mass spectrometer (C-ToF-AMS) (Aerodyne Research, Inc., Billerica, MA, USA), which is described in detail in the literature (Jayne et al., 2000; Jimenez et al., 2003; Drewnick et al., 2005; Canagaratna et al., 2007). In brief, particles are sampled through a 100 µm critical orifice (2 torr) and passed through an aerodynamic lens. The lens both focuses the particles into a narrow beam and accelerates them to a velocity dependant on particle vacuum aerodynamic diameter (d_{va}). The particles impact a resistively heated surface (600 °C, 10^{-7} torr) and flash-vaporize. The resulting gas is ionized by electron impact (70 eV) and the ions are detected by a time-of-flight mass spectrometer. The AMS may be operated in one of two modes: (1) The particle beam is alternately blocked and unblocked, yielding a full mass spectrum; or (2) The particle beam is modulated with a spinning chopper wheel (150 Hz), allowing determination of d_{va} from the particle time-of-flight between the chopper and detector. Because the mass spectrometer records spectra at 50 kHz, size-resolved mass spectra are obtained. The AMS used in this study was equipped with an optical scattering module, which provides a scattered light pulse for every particle impacting the vaporizer (Cross et al., 2007) above the optical detection limit of ∼215 nm (geometric diameter). Incorporation of this module into the ToF-AMS enables the quantitative detection of single particle mass spectra (Cross et al., 2009). Data presented in the manuscript body are taken exclusively from ensemble mass spectra (5 min average), however the size-resolved and single particle spectra are used to evaluate the instrument collection efficiency, as discussed below. Reported mass loadings are based on the standard pressure at the time of calibration.

An important consideration in the quantitative analysis of AMS data is the collection efficiency due to particle bounce. On impacting the vaporizer, some fraction of non-refractory particles bounces off the vaporizer surface instead of vaporizing. The detected number fraction is defined as the bounce collection efficiency (E_b), which depends primarily on particle phase (Matthew et al., 2008). Typically E_b ∼0.5 for ambient particles, although higher values have been obtained for acidic particles, particles with a high mass fraction of ammonium nitrate or liquid organics, and particles sampled at high relative humidity. Two methods were used to estimate E_b: (1) correlated optical scattering measurements and single particle mass spectra and (2) comparison of AMS and SMPS (scanning mobility particle sizer:

differential mobility analyzer (DMA) model 3071 coupled to a condensation particle counter (CPC) model 3010, TSI, Inc., St. Paul, MN, USA) data. The two methods are described in more detail below. The first method of E_b estimation was applied to all data collected beginning 25 May (when the optical scattering system became operational). The second method was applied to the entire study (14 May to 15 June). The two methods yielded similar results and E_b was estimated to be 0.6 ± 0.1.

E_b has traditionally been estimated through comparisons with co-located instrumentation. However, the combination of the optical scattering module and single particle mass spectra provides a direct in situ measurement of E_b as the fraction of light scattering pulses that contain a correlated chemical ion signal for particles larger than the 215 nm detection limit (Cross et al., 2008). We assume that the measured E_b for this particle subset extends across the entire size range to obtain a global estimate of E_b.

A second estimate of E_b was obtained through comparison of the AMS mass distributions with volume distributions from an SMPS, which measured mobility size distributions on a 15 min time interval for particles with mobility diameters (d_m) below 400 nm. AMS distributions were converted from mass to volume for each 15 min interval by the relationship $d_{va} = d_m \cdot \frac{\rho_p}{\rho_0} \cdot \frac{1}{\chi^2}$, where d_m is the SMPS-measured mobility diameter, ρ_p and ρ_0 are the particle and unit densities, respectively, and χ is the dynamic shape factor. For this conversion, we assumed spherical particles (i.e. χ = 1) and component densities of 1.77 g cm^{-3} for sulfate, 1.74 g cm^{-3} for nitrate, 1.527 g cm^{-3} for chloride, a weighted average of the sulfate and nitrate densities for ammonium, and 1.2 g cm^{-3} for organics. The AMS and SMPS volume distributions were compared below the SMPS large-size cutoff of d_m=400 nm.

In this manuscript, we report the AMS time series of potassium, measured at *m/z* 39. Because previous studies using the high-resolution HR-ToF-AMS have shown the *m/z* 39 signal to be dominated by $C_3H_3^+$ (Aiken et al., 2009), a further description of this measurement is required. Although the C-ToF-AMS is primarily a unit resolution mass spectrometer, in the present study sufficient resolution exists to distinguish the signals at K^+ (*m/z* 38.9637) and $C_3H_3^+$ (*m/z* 39.0235). Spectra were analyzed using the PIKA v1.06A software (D. Sueper, U. of Colorado-Boulder, USA) (DeCarlo et al., 2006). The time series of K^+ and $C_3H_3^+$ are presented in the Supplement (Fig. S1 http://www.atmos-chem-phys.net/10/2825/2010/acp-10-2825-2010-supplement.pdf). A relative ionization efficiency (RIE) of 10 was estimated for potassium from calibration with KNO_3 (where RIE is defined in reference to the signal at *m/z* 30 and 46 for NO_3 ion fragments). This value is notably higher than a previously reported potassium RIE = 2.9 (Drewnick et al., 2006). However, significant variation between instruments is expected because of the effects of mass spectrometer tuning on the sampling efficiency of ions from surface ionization. The potassium measurement presented here should be considered only semi-quantitative due to (1) the low mass resolution of the C-ToF, (2) the high instrument background at *m/z* 39, and (3) competition between multiple ionization processes.

2.2.2 Cloud condensation nucleus counter

Cloud condensation nuclei (CCN) concentrations were measured using a home-built CCN counter (Kumar et al., 2003) consisting of a coupled continuous flow thermal gradient diffusion chamber (TGDC) and aerodynamic particle sizer (APS) model 3320 (TSI, Inc., St. Paul, MN, USA). The chamber supersaturation was calibrated using size-selected $(NH_4)_2SO_4$ particles and was set at 0.42% for the present experiments. CCN number concentrations are measured to within $\pm$ 25%. Further details of instrument calibration, performance, and operation are available in the literature (Kumar et al., 2003; Chang et al., 2007, 2009).

2.2.3 Gas measurements

Volatile organic compounds (VOCs) were measured using a proton-transfer reaction mass spectrometer (PTR-MS) (Lindinger et al., 1998; de Gouw and Warneke, 2007) (Ionicon Analytik, Innsbruck, Austria) and a gas chromatography system coupled to a flame ionization detector system (GC-FID) (Brickell et al., 2003; Rupakheti et al., 2005). In the PTR-MS, H_3O^+ ions are generated by a cathode discharge in water vapor and ionize trace gases that have a higher proton affinity than water. The resulting ions are detected with a quadrupole mass spectrometer. Because this soft ionization technique causes relatively little fragmentation, measured *m/z*'s can frequently be directly related to the parent ion, and VOCs identified. The PTR-MS was calibrated with a custom standard containing 12 VOC species (methanol, acetonitrile, acetone, isoprene, methyl vinyl ketone, benzene, toluene, acetaldehyde, dimethylsulfide, α-pinene, limonene, 2-methyl-3-buten-2-ol) in the 500 ppbv range (Apel-Riemer Environmental Inc., Broomfield, CO, USA). Species-dependent calibration factors and detection limits are described elsewhere (Vlasenko et al., 2009). The GC-FID system employs a liquid nitrogen-cooled glass bead pre-concentration trap and multi-column capillary chromatography system. The instrument has detection limits of 5–16 pptv in an air sampling volume of 930 mL and was validated in a recent intercomparison study (Rappenglück et al., 2006). Gaseous CO and NO_x were measured using a TECO 48C and TECO 42C, respectively (Thermo Electron Corporation, Waltham, MA, USA).

2.3 Positive matrix factorization (PMF)

The AMS organic mass spectra were analyzed using positive matrix factorization (PMF) (Paatero and Tapper, 1994; Paatero, 1997), a receptor modeling technique that uses multivariate statistical methods to represent the time series of mass spectra as a linear combination of factor mass spectra

and their time-dependent intensities. PMF analysis was performed using the PMF2 software package (P. Paatero, U. of Helsinki, Finland), together with the CU AMS PMF Tool (Ulbrich et al., 2009a). The PMF model is described by the matrix equation:

$$\mathbf{X} = \mathbf{GF} + \mathbf{E} \quad (1)$$

Here **X** is the input mass spectral time series, the columns of the **G** matrix contain the factor time series and the rows of the **F** matrix contain the factor mass spectra. The **E** matrix contains the residuals and is defined by Eq. 1. The PMF model solves Eq. 1 by using a weighted least-squares algorithm to minimize the quantity Q, defined as:

$$Q = \sum_i \sum_j \left(e_{ij}/s_{ij}\right)^2 \quad (2)$$

Here e_{ij} are the elements of the residual matrix **E**, and s_{ij} are the elements of the uncertainty matrix **S**. The theoretical value of Q, denoted Q_{expected}, can be estimated as the number of elements in the input matrix **X**. In practice, Q is expected to be somewhat larger than Q_{expected} for ambient data because the data cannot be perfectly represented by a finite number of factors.

The AMS uncertainties (s_{ij}) discussed in Eq. 2 are calculated from the convolution of a Poisson distribution representing ion counting statistics with a detector-dependent Gaussian distribution representing the variation in single ion signal intensity (Allan et al., 2003). Uncertainties are calculated independently for the background and particle beam and summed in quadrature, yielding the expression $\Delta I_d = \alpha \frac{\sqrt{I_o + I_b}}{\sqrt{t_s}}$. Here I_o and I_b are the ion signals in the unblocked and blocked (background) positions, t_s is the sampling time, and α is a factor accounting for the width of the Gaussian distribution discussed above. The elements of the uncertainty matrix **S** are the ΔI_d values for each individual *m/z* at every point in time.

The PMF2 software was applied to a mass spectral matrix consisting of the organic component of all *m/z*'s $\leq$300, yielding a mass spectral matrix of 270 *m/z*'s and 8143 mass spectra (not all *m/z*'s contain organic signal). The PMF2 "robust" operating mode was utilized, in which data points yielding large residuals ($|e_{ij}/s_{ij}| > 4$) are iteratively downweighted (Paatero, 1997). Matrix rotations were explored by varying the *fPeak* parameter from -1.5 to 1.5 (see Fig. S7) and provided results consistent with those presented below (obtained at *fPeak* = 0.0). The possibility of local minima in the solution space was considered by initiating the PMF2 routine from 100 random starting points, denoted by seed values from 1 to 100. The different seed values yielded similar solutions to those presented below (obtained at seed = 1), indicating that other local minima were not found (see Fig. S8). Selection of the correct number of factors, as well as factor identification, is discussed in Sect. 3.1.1.

2.4 AURAMS (A Unified Regional Air-quality Monitoring System) Model

AURAMS (version 1.4.0) is an off-line chemical transport model (CTM) that is driven by the Canadian operational weather forecast model, GEM (Global Environmental Multiscale model) (Côté et al., 1998a, b). GEM (version 3.2.2) was used to produce meteorological fields with a 15-km horizontal resolution. GEM was run for 12-h periods from reanalysis files with a 6-h spin-up and 6 h of simulation stored for the CTM. AURAMS was run in a one-way nested configuration with a continental-scale outer domain at 42-km resolution and an inner regional domain at 15-km resolution.

Hourly anthropogenic point, area, and mobile emission files were prepared for the CTM using the 2005 Canadian and 2005 US emissions inventories and version 2.3 of the SMOKE emissions processing system (Houyoux et al., 2000; CEP, 2003). Biogenic emissions were calculated on-line by AURAMS using BEIS version 3.09, the Biogenic Emissions Landcover Database (BELD3) vegetation data set (30 tree species and 20 crop species used for Canada), and meteorological fields (temperature and irradiance) from GEM. Biogenic VOC emissions are speciated into four groups: isoprene (ISOP), monoterpenes (PINE), sesquiterpenes (SESQ) and "other VOCs". Sesquiterpene emissions were calculated by scaling monoterpene emissions (Helmig et al., 2007) (e.g. SESQ emissions equal to 0.16 times monoterpene emissions at 30 °C).

The gas-phase mechanism in AURAMS is an updated version of the ADOM-II mechanism (Kuhn et al., 1998), which is solved using a vectorized version of the rodas3 solver (Sandu and Sander, 2006). A detailed description of the ADOM-II VOC lumping scheme is presented elsewhere (Stroud et al., 2008). In the present study, a lumped monoterpene species was separated from the original ADOM-II anthropogenic long-chain alkene species and assigned the $OH/O_3/NO_3$ kinetics of α-pinene. A lumped sesquiterpene species was added to the mechanism and modeled with β-caryophyllene + O_3/OH/NO_3 kinetics. Benzene was separated from the original ADOM-II lumped species (sum of propane, acetylene, and benzene), and reacted in the modified mechanism with OH kinetics. The overall organic aerosol yield approach (Odum et al., 1996) was applied to the following VOC precursor species: isoprene (ISOP), monoterpenes (PINE), sesquiterpenes (SESQ), benzene (BENZ), mono-substituted aromatics (TOLU), multi-substituted aromatics (AROM), long chain anthropogenic alkenes (ALKE), and long chain anthropogenic alkanes (ALKA). Aerosol yields were calculated for low and high NO_x limits as a function of existing organic aerosol loadings (including both primary and secondary aerosol) and temperature. SOA yields are based on on Raoult's law equilibrium for an ideal solution composed of both POA and SOA (Pankow, 1994). Updated α_i and K_i based on recent literature studies were applied for ISOP (Kroll et al., 2006; Lane

et al., 2008), PINE (Griffin et al., 1999; Zhang et al., 2006; Pathak et al., 2007), SESQ, ALKE, and ALKA (Lane et al., 2008), BENZ and AROM (Ng et al., 2007b), and TOLU (Hildebrandt et al., 2009). An incremental increase in SOA mass was calculated from decreases in precursor VOC concentrations for a given time step under both low and high NO_x conditions. A linear interpolation between the low NO_x and high NO_x incremental SOA mass was performed based on the fraction of the RO_2 radicals which react with HO_x vs. NO_x (Presto and Donahue, 2006; Henze et al., 2008).

An SOA material density of $1.5\,g\,cm^{-3}$ was assumed for conversion of normalized aerosol yield data (from particle volume measurements); recent volatility basis sets have used 1.6 and $1.4\,g\,cm^{-3}$(Shrivastava et al., 2008; Tsimpidi et al., 2010). (Note that this value for the SOA material density is distinct from the assumed density of $1.2\,g\,cm^{-3}$ for the total organic fraction used in the AMS collection efficiency estimation; see Sect. 2.2.1.) The particle size distribution is represented in the CTM by 12 bins ranging in diameter from 0.01 to 40.96 µm, with the 8 lower bins corresponding to sizes below 2.5 µm. Particle composition is represented by nine species (sulfate, nitrate, ammonium, black carbon, primary organic aerosol, SOA, crustal material, sea salt, and particulate water), which are assumed to be internally mixed within each size bin (Smyth et al., 2009). Condensation of the SOA to the particle size distribution is described by a modified Fuchs-Sutugin equation as described by equation A14 in Gong et al. (Gong et al., 2003).

2.5 Remote sensing

The spatial and temporal domain of this analysis is extended using satellite observations from the Moderate Resolution Imaging Spectroradiometer (MODIS) onboard the Terra satellite. MODIS/Terra has taken global daily measurements of solar backscatter at 10:30 AM local time since mid-2000. The retrieval of aerosol optical depth (AOD), a measure of light extinction by aerosol in the atmospheric column, is described in the literature (Remer et al., 2005; Levy et al., 2007). Validation of the retrieved AOD with ground-based AERONET observations yields a typical accuracy of $0.05 \pm 15\%$ (Remer et al., 2005). We use here Collection 5 level 2 quality 3 data. The MODIS fire count algorithm, available from the USDA Forest Service, Remote Sensing Applications Center, uses brightness temperature from the MODIS 4 µm and 11 µm channels to detect the presence of fire (Giglio et al., 2003).

For the Egbert site, MODIS AOD is compared with AOD obtained from AERONET (Aerosol Robotic Network) measurements. AERONET is a globally distributed network of CIMEL spectral radiometers. Version 2, level 2 data is utilized for this analysis. AERONET AOD retrievals have an uncertainty of 0.01 to 0.02 (Holben et al., 2001).

3 Results and discussion

3.1 AMS organic mass spectral analysis

3.1.1 Positive matrix factorization

The application of PMF to an AMS dataset has been previously described in detail (Lanz et al., 2007; Ulbrich et al., 2009a; Slowik et al., 2010). An important consideration is the number of factors output by the PMF algorithm, which is selected by the user. However, no completely unambiguous method for choosing the "correct" number of factors exists. The selected number of factors is thus somewhat subjective and must be evaluated through comparisons of factor and tracer time series, analysis of the factor mass spectra, and the evolution of the residual time series as a function of the number of resolved factors. Here a 4-factor solution was selected as the best representation of the data, as described below.

In Fig. 1, we plot the time series of the quantity $\Delta\left(\sum_j \left(e_{ij}/s_{ij}\right)^2\right)$ between two solutions with different numbers of factors: that is, the time-dependent contribution to Q for the n-factor solution minus that of the $(n+1)$-factor solution. The appearance of time series structure in such a plot indicates that the increased number of factors enables more of the data to be explained. Structure is evident in Fig. 1a–c, but is greatly reduced in Fig. 1d. (Note that the scale in Fig. 1a is ∼60x that of Fig. 1b and ∼120x that of Figs. 1c and d.) These trends in time series structure indicate that the PMF solution is enhanced by increasing the number of factors to 4, but that further improvements do not explain significantly more of the data.

As described below, the 4-factor solution contains factors identified as hydrocarbon-like organic aerosol (HOA), biomass burning organic aerosol (BBOA), and more- and less-oxygenated organic aerosol (denoted as OOA-1 and OOA-2, respectively), designations that result from correlations with tracer species and comparison with previous PMF analyses of AMS data, as discussed below. Increasing the number of factors to 5 yields a third OOA factor and alters the mass spectra and time series of the OOA-1 and OOA-2 factors (see Fig. S6). This is consistent with factor mixing/splitting behavior, previously identified as an indicator of an excessive number of factors (Ulbrich et al., 2009a). Further, the additional OOA factor does not aid the interpretation of the dataset. Given this lack of improvement in the $\Delta\left(\sum_j \left(e_{ij}/s_{ij}\right)^2\right)$ time series for the 5-factor solution, the absence of external tracer data supporting a 5-factor solution over the 4-factor, and the similarity of the 5-factor solution to known factor mixing/splitting artifacts observed in synthetic datasets at excessive number of factors (Ulbrich et al., 2009a), the 4-factor solution is considered optimal.

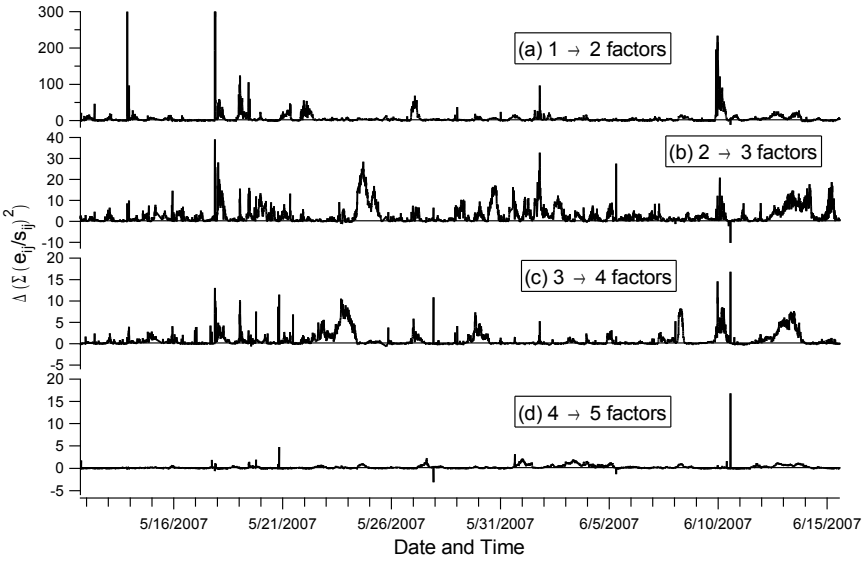

Fig. 1. Effect of the number of factors in the PMF solution on the time-dependent contribution to Q. The plotted quantity is the difference between the two cited solutions, i.e. Fig. 1a shows contribution to Q for the 1-factor solution minus that of the 2-factor solution.

3.2 Evaluation and analysis of AMS PMF factors

The factor mass spectra and time series for the 4-factor PMF solution are plotted in Fig. 2. Figure 2b also shows the time series of tracer species correlated with the PMF factors. Factor mass spectra are normalized such that the sum of each spectrum across all *m/z* is equal to 1. The factor time series are reported in units of mass concentration ($\mu g\,m^{-3}$). A brief discussion of the factor mass spectra and time series is presented below. All comparisons with previously reported spectra were performed using spectra obtained from the AMS Spectral Database (Ulbrich et al., 2009b).

The mass spectrum of the HOA factor (F1) correlates with that of HOA factors obtained in other locations (e.g. R^2 = 0.78 vs. Pittsburgh HOA (Zhang et al., 2005), R^2 = 0.54 vs. Zurich summer HOA (Lanz et al., 2007), and R^2 = 0.68 vs. Zurich winter HOA (Lanz et al., 2008). The primary difference between the previously reported HOA spectra and Egbert HOA is that the Egbert HOA has more signal at low *m/z*'s, particularly *m/z* 15, 27, and 29. These three *m/z*'s comprise 15.3% of the spectrum vs. 4.4% to 7.8% in previous studies. Similar to previous studies (Lanz et al., 2007; Ulbrich et al., 2009a; Slowik et al., 2010), the HOA time series correlates with tracers of primary anthropogenic emissions, such as NO_x (R^2 = 0.41) and benzene (R^2 = 0.43) as shown in Fig. 2b. Differences between the HOA, NO_x, and benzene time series are likely governed by changes in emissions profiles, e.g. the relative contributions of the Toronto plume vs. highway emissions to the east/southeast.

The BBOA factor mass spectrum (Fig. 2a) is the only resolved factor containing significant signal at *m/z* 60 and 73. These fragments are characteristic of levoglucosan, a tracer for cellulose pyrolysis. The BBOA mass spectrum correlates both with that of levoglucosan (Schneider et al., 2006) (R^2 = 0.70) and a Zurich wood-burning PMF factor (Lanz et al., 2007) (R^2 = 0.80). In Fig. 2b, the BBOA time series is plotted together with the semi-quantitative AMS measurement of potassium (R^2 = 0.30) and PTR-MS measurement of acetonitrile (R^2 = 0.34). Only qualitative correlations are expected because (1) the BBOA factor is not a conserved tracer for primary emissions and (2) the potassium and acetonitrile measurements are both somewhat problematic. As fresh biomass burning emissions are photochemically processed, conversion of BBOA-like spectra to OOA-like spectra have been observed in both biomass burning plumes (Capes et al., 2008) and chamber experiments (Grieshop et al., 2009b). The potassium measurement issues were discussed in Sect. 2.2.1. Recent high resolution PTR-MS measurements in downtown Toronto indicate an interference at *m/z* 42 from the $C_2H_2O^+$ ion (A. Vlasenko, personal communication, 2009). This likely influences the acetonitrile time series during periods of Toronto outflow; its effect at other times is unknown.

The mass spectrum and time series of the more oxygenated OOA factor, denoted "OOA-1," are shown in Figs. 2a and b, respectively. Relative oxygenation is inferred from the ratio of *m/z* 44 (CO_2^+ ion) to the total mass spectrum. For OOA-1, the 44/total ratio is 0.19 (vs. 0.10 for the less oxygenated OOA-2). These values correspond to O/C ratios of ∼0.81 (OOA-1) and ∼0.46 (OOA-2) based on the approximation presented by Aiken et al. (2008). Increased oxygenation is expected to correlate with increased particle age (Lanz et al., 2007; Aiken et al., 2008; Ulbrich et al., 2009a) and decreased volatility (Huffman et al., 2009). The OOA-1 mass spectrum closely resembles that of OOA factors extracted

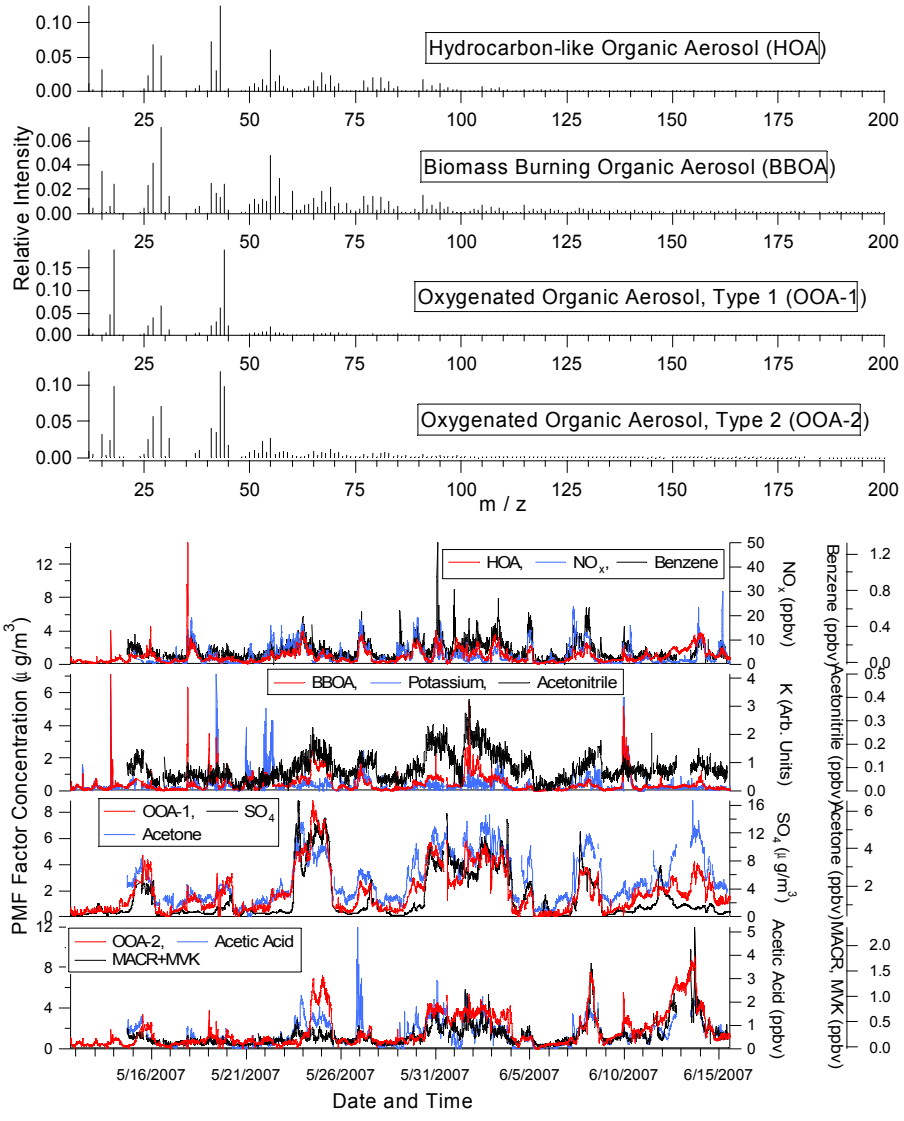

Fig. 2. Factor mass spectra **(a)** and time series **(b)** for the 4-factor solution to the AMS dataset. Mass spectra are normalized such that the sum of each spectrum across all *m/z*'s is equal to 1. Time series are plotted for both AMS PMF factors (red traces, left axis) and selected tracer species (black and blue traces, right axis).

from AMS measurements in several locations (e.g. $R^2 = 0.88$ with vs. Pittsburgh OOA (Zhang et al., 2005). As shown in Fig. 2b, the time series of OOA-1 correlates with AMS measurements of particulate sulfate ($R^2 = 0.77$), which is mostly attributed to long-range transport, and acetone ($R^2 = 0.70$), a long-lived oxygenated VOC generated in part through photochemical reactions (Vlasenko et al., 2009).

Unlike the OOA-2 factors previously extracted from AMS datasets in Zurich and Pittsburgh (Lanz et al., 2007; Ulbrich et al., 2009a) where volatility is thought to drive the factor time series, Egbert OOA-2 does not correlate with particulate nitrate (not shown). Instead, Egbert OOA-2 correlates with VOC photochemical products. This is shown in Fig. 2b, where the OOA-2 time series is plotted together with that of PTR-MS *m/z* 71, which is attributed to methacrolein (MACR) and methyl vinyl ketone (MVK). These VOCs are photochemically generated and have lifetimes on the order of half a day (Biesenthal et al., 1998). OOA-2 also correlates with acetic acid (at PTR-MS *m/z* 61), a longer-lived product of VOC oxidation. Similar correlations are also observed with formaldehyde, acetone, and a factor obtained from PMF analysis of the PTR-MS spectrum (Vlasenko et al., 2009). In addition to the species already mentioned, the PTR-MS PMF factor includes the majority of the signal assigned to *m/z* 99 (pinonaldehyde fragment), *m/z* 113 (attributed to monoterpene oxidation products in chamber studies) (Lee et al., 2006a, b), and a number of other peaks expected to correspond with oxygenated compounds.

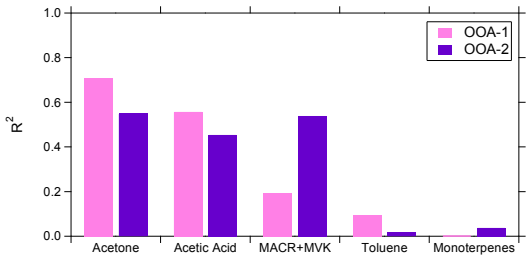

Fig. 3. Correlations between the time series of OOA-1 and OOA-2 factors with selected VOCs over the entire study period.

The OOA-1 and OOA-2 factor mass spectra are similar to those of low-volatility OOA (LV-OOA) and semivolatile OOA (SV-OOA), respectively (Jimenez et al., 2009). Based on these spectral similarities and the lower O:C ratio of OOA-2, it is likely that OOA-2 constitutes the more volatile OOA fraction. However, as noted above, this cannot be directly supported by analysis of the time series. Because tracer correlations suggest that the Egbert time series are primarily driven by factors other than volatility, the more general OOA-1/OOA-2 terminology is used in this manuscript.

The relative age of the OOA-1 and OOA-2 factors can be inferred through the correlations of these factors with VOCs having known atmospheric lifetimes. Figure 3 shows the R^2 values for correlations of OOA-1 and OOA-2 with acetone, acetic acid, MACR+MVK, toluene, and monoterpenes over the entire study period. As expected, neither factor correlates with toluene and monoterpenes. Both factors correlate with acetone, acetic acid, and MACR+MVK. However, OOA-2 correlates more strongly with MACR+MVK (lifetime of approximately half a day (Biesenthal et al., 1998) than does OOA-1. In contrast, OOA-1 correlates more strongly with the longer-lived acetone and acetic acid (lifetime of days to weeks) than does OOA-2. The trends in these correlations indicate that (1) OOA-2 results from more recent oxidation than OOA-1, and (2) a large fraction of OOA-2 is formed within half a day (i.e. before MACR+MVK is destroyed). Note that the weak correlation of OOA-1 with MACR+MVK suggests that a lesser fraction of OOA-1 is also generated on this timescale.

3.3 Identification and characterization of biogenic period

Figure 4 shows the time series of measured particulate inorganic species, organic factors from the PMF analysis, and selected VOCs. The dashed backgrounds in Fig. 4 denote three case study periods selected for contrasting analysis of biogenic influences (9 June to mid-day on 13 June), urban outflow (30 May to 3 June), and biomass burning (evening on 9 June to mid-morning on 10 June).

The biogenic period corresponds with steadily increasing temperatures under clear sky conditions, with back trajectories (presented later in Fig. 10c) and surface wind direction indicating air transported from north of the site. During this period, the organic aerosol mass builds steadily, with local maxima in the afternoons of 11, 12 and 13 June. A corresponding increase is evident in the photochemical reaction products MACR and MVK. Acetylene (a long-lived anthropogenic tracer) mixing ratios remain very low. This behavior contrasts sharply with the elevated acetylene mixing ratios observed during periods of urban outflow from the south (e.g. 23 to 25 May, 30 May to 4 June, 7 to 8 June). Monoterpene mixing ratios are elevated during the 9 to 13 June period; however, monoterpene lifetimes (a few hours) are sufficiently short that a strong correlation with organic aerosol mass may not be expected. The particle composition is perturbed during the biogenic period by: (1) a plume from smelting operations in Sudbury, Ontario (∼300 km to the north), leading to increased sulfate (overnight 11–12 June); and (2) a biomass burning event during the first half of 10 June.

The anthropogenic case study is characterized by southerly winds. Back trajectories indicate air masses passing over the Toronto urban area and populated regions to the south/southwest. Aromatic VOCs, NO_x, and particulate sulfate are all elevated. The high sulfate periods on 15 May, 24–25 May, and 9 June are examples of similar events, though of shorter duration.

The biomass burning period is characterized by high potassium and slightly elevated acetonitrile. BBOA concentrations are near their maximum for the study period. While potassium, acetonitrile, and BBOA are elevated and correlated at other periods during the study, this occurs during periods strongly influenced by anthropogenic emissions, making them unsuitable for examination of biomass burning aerosol.

As shown in Fig. 4, the organic composition during the biogenic event is characterized by increased OOA-2 relative to OOA-1 and very low BBOA and HOA. During the biogenic event, OOA-2 constitutes 65% ± 10% of the total OOA (i.e. OOA-1 + OOA-2), vs. 46% ± 5% during periods of urban outflow (e.g. 30 May to 3 June) (reported uncertainties are the standard deviation of the OOA-2/organic mass fraction). As discussed in the previous section, the correlation of OOA-2 with MACR+MVK during the biogenic period (R^2 = 0.71) indicates that the organic aerosol during the biogenic period is relatively fresh and therefore not the result of highly processed anthropogenic or biomass burning emissions. In contrast, OOA-1 is more strongly correlated with longer-lived photochemical oxidation products such as acetone, while HOA and BBOA correlate with tracers of primary emissions.

The biogenic period is distinguished by the relationship between the total organic material (OM) and OOA components with the CO mixing ratio, which are plotted against each other in Fig. 5 for the biogenic, biomass burning, and urban outflow periods identified in Fig. 4. CO is a

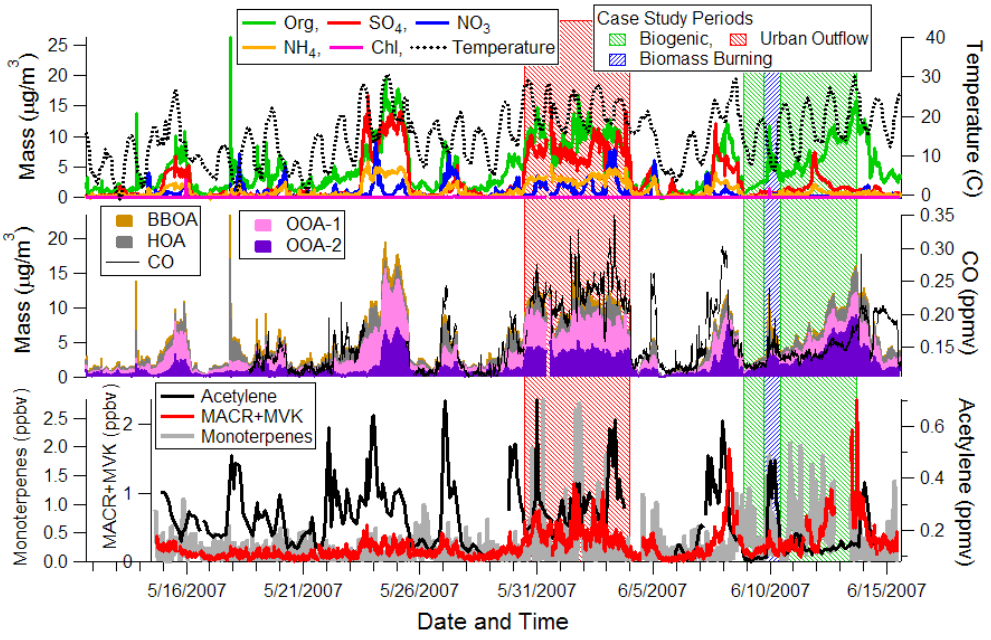

Fig. 4. Time series of AMS measurements (top panel), AMS PMF factors (middle panel), and selected gas-phase species (bottom panel). Mixing ratios of methacrolein and methyl vinyl ketone (MACR+MVK) and monoterpenes are obtained from the PTR-MS measurements at *m/z* 71 and 137, respectively. Acetylene is obtained from GC-FID measurements.

long-lived species (lifetime on the order of a few months) that enters the atmosphere by direct emission from primary combustion and by gas-phase photochemistry, such as photolysis or OH-oxidation of formaldehyde. Figure 5a shows a dramatic difference in $\Delta OM/\Delta CO$ between the biogenic period (234.4 $\mu g\,m^{-3}\,ppmv^{-1}$) vs. the urban outflow and biomass burning periods (71.1 $\mu g\,m^{-3}\,ppmv^{-1}$ and 109.1 $\mu g\,m^{-3}\,ppmv^{-1}$, respectively). Previous measurements of $\Delta OM/\Delta CO$ in anthropogenically-influenced regions (shaded region of Fig. 5a) have yielded values in the range of 10 to 85 $\mu g\,m^{-3}\,ppmv^{-1}$, with higher values corresponding to increased photochemical age (de Gouw et al., 2008; DeCarlo et al., 2008; Kleinman et al., 2009). The Egbert urban outflow case study is consistent with these values. Previous measurements of $\Delta OM/\Delta CO$ in fresh and aged biomass burning plumes are presented in Table 1; values from the biogenic, biomass burning, and urban outflow case studies are included for comparison. The Egbert biomass burning case study is consistent with previous measurements of fresh biomass burning emissions. We note that none of the values in this table are from boreal fire emissions, however yellow pine combustion (Grieshop et al., 2009) may be a reasonable surrogate.

The biogenic $\Delta OM/\Delta CO$ in Fig. 5a is clearly distinct from from previous measurements of fresh biomass burning emissions and urban outflow (as well as the biomass burning and urban outflow case study periods). As is evident from Table 1, there are significant uncertainties in the effect of atmo-

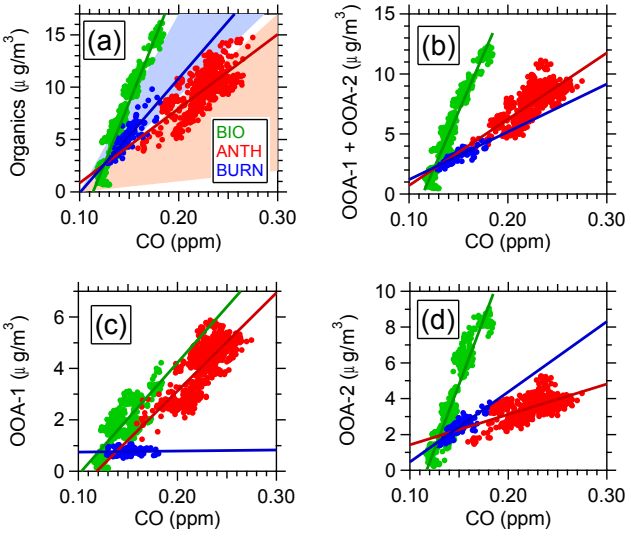

Fig. 5. Mass concentration of **(a)** total organics, **(b)** OOA-1 + OOA-2, **(c)** OOA-1, and **(d)** OOA-2 as a function of CO for selected periods dominated by biogenic (green), anthropogenic (red), and biomass burning (blue) sources. The red shaded region in Fig. 5a denotes the range of previously observed values for $\Delta OM/\Delta CO$ for anthropogenically-influenced regions (de Gouw et al., 2008; DeCarlo et al., 2008; Kleinman et al., 2009). Literature values for biomass burning are presented in Table 1.

Table 1. Comparison of literature ΔOM/ΔCO values for fresh and aged biomass burning with case study periods in the present study (see Figs. 4 and 5a).

Study	ΔOM/ΔCO ($ug\,m^{-3}\,ppm^{-1}$)	Description
Fresh Emissions		
(Capes et al., 2008)	51	West African Sahel
(DeCarlo et al., 2008)	80	Mexico City plumes influenced by fires
(Grieshop et al., 2009)	2.1 to 6.9	Laboratory: laurel oak
(Grieshop et al., 2009)	1.4 to 77	Laboratory: yellow pine
(Yokelson et al., 2007a)	121	Amazon fires (PM_{10})[a]
(Yokelson et al., 2007b)	91	Forest fires near Mexico City ($PM_{1.0}$)[a]
(Yokelson et al., 2009)	33.0 to 49.8	Yucatan fires
Aged Emissions		
(Capes et al., 2008)	51	West African Sahel
(Grieshop et al., 2009)	4.0 to 14	Laboratory: laurel oak
Grieshop et al., 2009)	3.6 to 200	Laboratory: yellow pine
Yokelson et al., 2009)	171	Yucatan aged smoke at 2476 m, $PM_{1.0}$
This Study (Fig. 5)		
Urban outflow case study	71.1	
Biomass burning case study	109.1	
Biogenic case study	234.4	

[a] Estimated from non-speciated PM measurements, assuming that OM accounts for 55% of PM (Reid et al., 2005).

spheric processing on the ΔOM/ΔCO ratio on biomass burning emissions. A constant value of $51\,\mu g\,m^{-3}\,ppm^{-1}$, independent of airmass age, was observed for fires in the West African Sahel (Capes et al., 2008). On the other hand, some studies indicate the ΔOM/ΔCO value may increase due to atmospheric processing (Grieshop et al., 2009; Yokelson et al., 2009). To our knowledge, the highest reported value is $200\,\mu g\,m^{-3}\,ppm^{-1}$, from laboratory aging of yellow pine (flaming with embers; other burn conditions yielded much lower values) (Grieshop et al., 2009). Thus the previously reported ΔOM/ΔCO for both fresh and aged biomass burning emissions are lower than that observed during the biogenic case study ($234.4\,\mu g\,m^{-3}\,ppm^{-1}$). Due to the large observed variations in source emissions profiles and atmospheric processing, the possibility that aged biomass burning emissions could approach the measured biogenic ΔOM/ΔCO ratio cannot be completely ruled out. However, the combination of the high ΔOM/ΔCO with other observations suggest that biomass burning does not significantly affect the OM during the biogenic period, as discussed in Sect. 3.3.3.

Figures 5c and d demonstrate that the difference in ΔOM/ΔCO between the biogenic and anthropogenic periods is driven by OOA-2. While ΔOOA-I/ΔCO is similar for the urban outflow and biogenic periods ($38.2\,\mu g\,m^{-3}\,ppmv^{-1}$ vs. $43.5\,\mu g\,m^{-3}\,ppmv^{-1}$), ΔOOA-2/ΔCO is highly source-dependent (anthropogenic: $17.0\,\mu g\,m^{-3}\,ppmv^{-1}$ vs. biogenic: $145.6\,\mu g\,m^{-3}\,ppmv^{-1}$). The biomass burning period is distinct from either period, with OM dominated by BBOA. The biomass burning ΔOOA-2/ΔCO ($39.2\,\mu g\,m^{-3}\,ppmv^{-1}$) more closely resembles urban outflow, while biomass burning OOA-1 remains at low, near-constant levels independent of CO (ΔOOA-I/ΔCO = $0.4\,\mu g\,m^{-3}\,ppmv^{-1}$). The tight correlation between OOA-2 and CO for the biomass burning and biogenic periods in Figure 5d suggests a relatively constant photochemical age. These correlations, coupled with the lack of intermediate points between the ΔOOA-2/ΔCO lines for the biomass burning and biogenic periods as would arise with changes to the emissions profile or photochemical environment, indicate that the organic concentrations during the biogenic period cannot be explained by aged biomass burning emissions. Further discussion of potential biomass burning influences is presented in Sect. 3.3.3. The distinct ΔOOA-2/ΔCO relationships described above suggest that OOA-2 observed during the biogenic period can be identified as biogenic SOA. As discussed in the following section, CO concentrations during the biogenic period are consistent with a photochemical source, suggesting that the high ΔOOA-2/ΔCO values likely result from the absence of a significant source of primary CO. The ΔOOA-2/ΔCO values are also affected by partioning and source proximity, although the diffuse nature of the biogenic VOC source may somewhat diminish these effects. The identity of the OOA-1 source is more ambiguous, due to its increased age and similarity of ΔOOA-I/ΔCO between the biogenic and anthropogenic periods. We therefore estimate the biogenic

SOA concentration as bounded by that of OOA-2 and OOA-1 + OOA-2, yielding a peak biogenic SOA concentration of 8 to 12 $\mu g\,m^{-3}$.

3.4 Model interpretation of the biogenic period

3.4.1 Photochemical CO production

The difference in $\Delta OOA/\Delta CO$ slopes can be understood in terms of the differences in CO sources and production mechanisms. CO is likely dominated by primary emissions during the anthropogenic period; however such emissions are expected to be negligible during the biogenic period. Instead, the strong correlation of CO with OOA-II, which during this period is correlated with the photochemical products MACR+MVK, suggests a photochemical source. The mass yield of SOA from biogenic VOCs can be estimated from Fig. 5, as discussed below. We assume all CO above the global background during the biogenic period is photochemical. A chemical transport model for the study region predicts average enhancements due to biogenic processes of at least 25 ppbv in mid-summer (Hudman et al., 2008). This is comparable to the observed CO increase of 60 ppbv determined from Fig. 5 as the difference between the maximum CO concentration and the x-intercept for the biogenic period. We believe our results show the first direct observational evidence for a significant biogenic source of CO from coniferous forests. This is consistent with a model/measurement comparison suggesting a major contribution of biogenic VOCs to the total CO budget for the continental United States during summer (Miller et al., 2008).

The relationship of CO to biogenic VOC mixing ratios is calculated using a box model, with α-pinene selected as a surrogate for precursor VOCs. (As discussed later in Sect. 3.3.2, the AURAMS air quality model identifies monoterpenes as the dominant precursor VOCs). A subset of a near-explicit Master Chemical Mechanism (v3.1) (Saunders et al., 2003) describing α-pinene oxidation (928 reactions and 310 compounds) is chosen. In order to run the model, 48 inorganic reactions and 21 inorganic compounds have been combined with that subset for α-pinene. More details of relevant model settings can be found in the literature (Xia et al., 2008). For simplicity, the chemistry is run in a zero-dimensional box model at a fixed temperature of 25 °C without deposition. The photolysis rates in the box model are set to the latitude of the Egbert site (44.23° N).

The chemical system was studied for 246 combinations of initial α-pinene concentrations and NO_x emission rates. Specifically, 6 different initial α-pinene concentrations (1.0 ppbv to 10.0 ppbv) and 41 different NO_x emission rates (1.8×10^5 molecules s^{-1} to 1.8×10^7 molecules s^{-1} yielding mean NO_x concentrations of 0.05 to 20 ppbv) were chosen, with the concentrations and emission rates selected to be evenly spaced on a logarithmic scale. During the biogenic period, the measured NO_x concentrations were 1.02 ± 0.74 ppbv, with a maximum of 4.72 ppbv (5 min average). The NO_x levels are increased by the Sudbury smelter plume (11 June), which increases NO_x and sulfate but does not significantly affect the organic concentration or composition. Excluding this period, NO_x concentrations were 0.78 ± 0.41, with a maximum value of 2.02 ppbv. These concentrations are slightly above the instrument detection limit ($\sim$0.2 ppbv). Because the Egbert site is located in a semirural rather than remote area, a small NO_x background is expected.

For each scenario, the model was run for 48 h from midnight, at which point the $\Delta CO/\Delta\alpha\text{-pinene}_{reacted}$ ratio is calculated. It is found that the obtained ratios lie within 3.0 ± 0.4. Results for the 48-h simulation are shown in Fig. 6. Beyond 48 h, the ratio continues to increase, reaching 3.4 ± 0.4, 3.8 ± 0.4, and 4.0 ± 0.4 at 72 h, 120 h, and 360 h, respectively.

As discussed in the previous section, we estimate the lower and upper limits of the biogenic SOA to be OOA-2 and OOA-1+OOA-2, respectively. The slopes of Figs. 5b and c, for the biogenic period yield $\Delta SOA/\Delta CO$ = 146 to 189 $\mu g\,m^{-3}\,ppmv^{-1}$. From the MCM 48-h simulation ($\Delta CO/\Delta\alpha$-pinene = 3.0 ± 0.4), this equates to $\Delta SOA/\Delta\alpha$-pinene of 437 to 567 $\mu g\,m^{-3}\,ppmv^{-1}$, or a mass yield of 7.2 to 9.3%. These values are consistent with the literature (indicating that the observed CO levels are consistent with a photochemical source), where reported SOA mass yields from α-pinene range from approximately 3 to 45%, although a direct comparison is complicated by the dependence of the yield on SOA mass loading (increased mass causes an increased yield), temperature, and high/low NO_x regimes (Griffin et al., 1999; Tunved et al., 2006; Ng et al., 2007a; Pathak et al., 2007; Shilling et al., 2008). Additionally, some production of CO and SOA from isoprene oxidation is expected. However, this is not expected to be a major source of either species because the airmass originates in the boreal forest. In this region, monoterpene and isoprene emissions are comparable (Stroud et al., 2008), while yields of SOA and CO from monoterpenes are much higher than from isoprene.

3.4.2 Regional SOA production

AURAMS (A Unified Regional Air-Quality Monitoring System) (Moran et al., 1998) model output for four subsequent days during the biogenic event (10 to 13 June) are plotted in Figs. 7 and 8. Figure 7 shows spatial distributions of $PM_{2.5}$ SOA, while Fig. 8 shows surface temperature and wind fields for the same time periods. The figures indicate generation of organic aerosol over forested regions of Ontario and Quebec correlated with increased temperature, followed by transport southwest to the Egbert site. Back trajectories indicate that air is transported between these locations over approximately a day. The observed elevated mixing ratios of MACR+MVK and monoterpene oxidation products at Egbert are consistent with this timescale, because MACR and MVK have

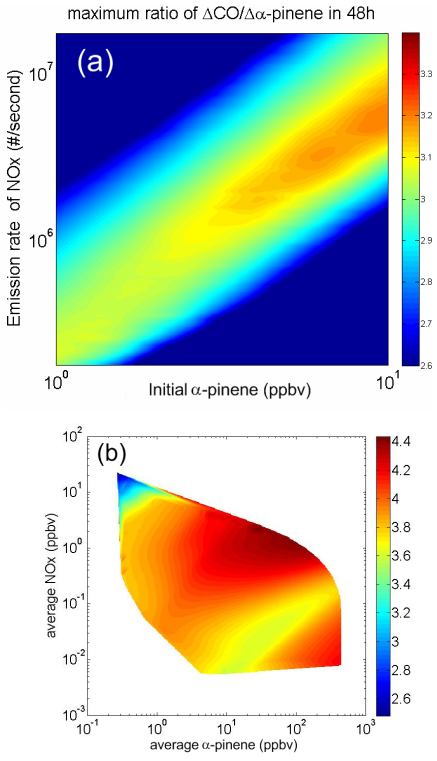

Fig. 6. Ratio of $\Delta CO/\Delta\alpha\text{-pinene}_{reacted}$ (colors) as a function of **(a)** NO_X emission rate and initial α-pinene concentration and **(b)** average NO_X and α-pinene mixing ratio for 48-h Master Chemical Mechanism model runs.

atmospheric lifetimes of approximately half a day (Biesenthal et al., 1998).

As shown in Fig. 9, the urban plume timing (7–9 June), smelter plume (sulfate, 12 June) and biogenic event (10–14 June) are well reproduced by AURAMS. The urban plume peak SOA concentration is underpredicted by AURAMS, consistent with other model/measurement comparisons in polluted regions (Johnson et al., 2006; Volkamer et al., 2006; de Gouw et al., 2008; Dzepina et al., 2009), although the relative contributions of fine-scale meteorology and SOA production to this discrepancy are uncertain. In contrast, the modeled and measured SOA concentrations for the biogenic event are in approximate agreement. Agreement between measured and modeled biogenic SOA has been recently observed in isoprene-dominated environments, although the possibility of cancelling errors cannot be discounted (Capes et al., 2009; Chen et al., 2009); as discussed below, the biogenic SOA at Egbert is more heavily influenced by monoterpene emissions.

We further note that the model/measurement agreement depends somewhat on the selected monoterpene yields from the literature. For our SOA model calculation, we have assumed our monoterpene model species to have an equal composition of α-pinene, β-pinene, and limonene (one-third each). We have used literature SOA yields from Pathak et al., (2007), Griffin et al., (1999) and Zhang et al. (2006) for the α-pinene, β-pinene, and limonene component, respectively. Compared to α-pinene, there are fewer SOA chamber studies for β-pinene, limonene and other monoterpenes that can be used to generate model SOA yield parameterizations. Recently, Shilling et al. (2008) observed dark-ozonolysis α-pinene yields in their continuous flow chamber that were approximately a factor of 1.5 to 2.0 higher than those in the Carnegie Mellon chamber (Pathak et al., 2007) and older Caltech chamber data (Griffin et al., 1999; Cocker et al., 2001). Such an increase in the α-pinene SOA yield leads to an approximate increase in the total SOA by a factor of 0.5 to 0.7 (i.e. 1.5/3 to 2.0/3), placing the AURAMS SOA between the OOA-2 and OOA-1 + OOA-2 estimates in Fig. 7. The observed agreement between model and measurements does not by itself indicate that all steps in the SOA model are resolved. Large uncertainties remain in the yields of monoterpene species (particularly those other than α-pinene) as well as the appropriate profile of monoterpene species (which varies with location). Thus the calculation may contain offsetting errors.

The sensitivity of SOA concentrations to individual classes of VOC precursors was tested in AURAMS by removing SOA production from these precursors (Fig. 9, lower panel). Removal of SOA production by monoterpenes, sesquiterpenes, and isoprene decreased SOA mass concentrations by 65%, 4%, and 7%, respectively. The high SOA concentrations during the biogenic event are therefore consistent with oxidation primarily from monoterpenes. Such an SOA source is consistent with regional biogenic VOC emissions. Isoprene and monoterpene mass emissions are comparable (within a factor of 2) (Stroud et al., 2008), while monoterpene SOA yields are roughly an order of magnitude larger. The inference of high biogenic SOA due to monoterpene oxidation is consistent with one other report in the literature of high biogenic SOA mass, which was also observed in a region of high terpene emissions (Shantz et al., 2004).

The degradation of the AMS/AURAMS agreement on 14 June is likely a reflection of model limitations with respect to capturing the fine-scale meteorological structure (vertical diffusion, deposition, horizontal transport). Such variation plays a large role in the fine-scale temporal differences between the model and measurements. The Egbert site experienced an abrupt change in wind direction (north to south) late on 13 June (i.e. the end of the biogenic period). Because Egbert is on the edge of the high regional SOA (see Fig. 7), this meteorology strongly influences the measurement/model agreement. The model/measurement divergence at the end of the period is thus likely caused by the model prediction of the location of the edge of the biogenic-influenced area.

The correlation between AMS measurements and AURAMS predictions of biogenic SOA in Fig. 9 suggest that the high loadings are due to high biogenic VOC emissions rather than unknown chemistry. Figure 8 shows temperatures in excess of 30 °C across a wide geographical area.

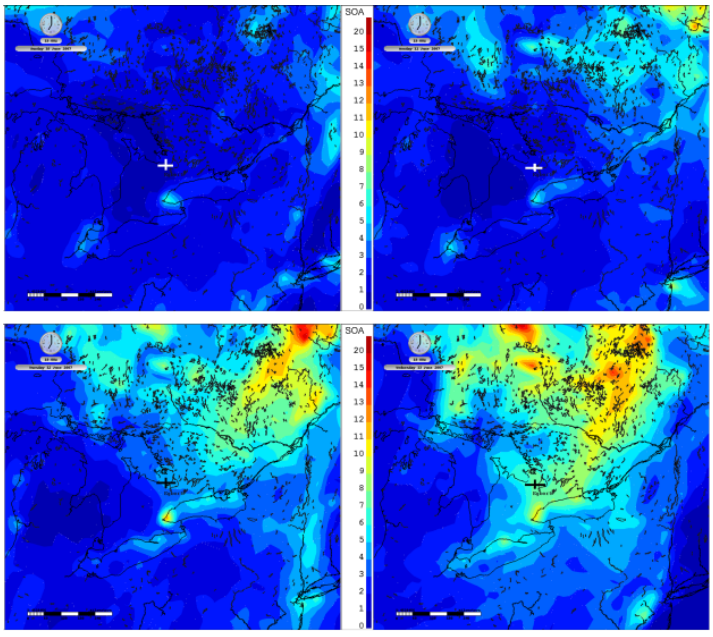

Fig. 7. Predicted PM2.5 SOA spatial distributions for the 42 km resolution grid. Images are for 19Z on 10, 11, 12, and 13 June. A cross marks the Egbert site. The color legend represents the mass concentration of SOA in $\mu g/m^3$.

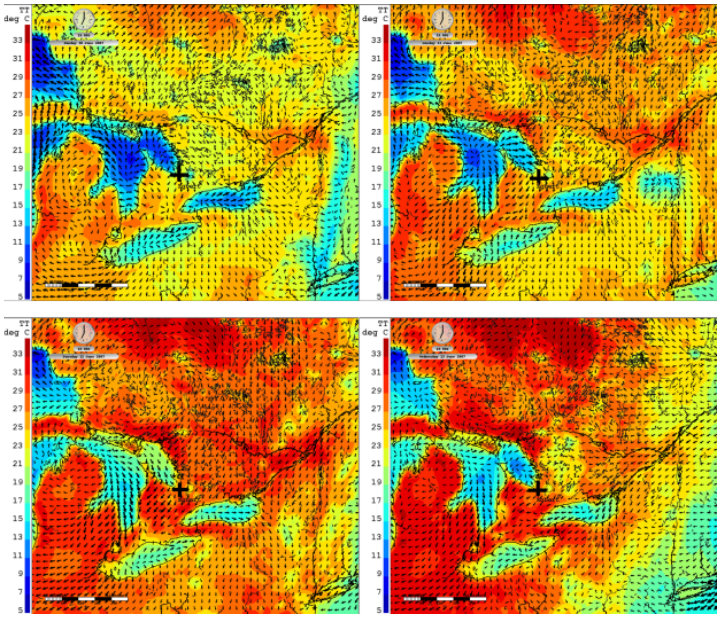

Fig. 8. Temperature and wind direction for the 15 km resolution nested grid. Images are for 19Z on 10, 11, 12, and 13 June. A cross marks the Egbert site. The color legend represents the temperature in °C. Arrows denote wind direction.

The regional biogenic SOA is expected to derive mostly from monoterpene precursors due to the combination of (1) comparable monoterpene and isoprene emissions rates (Stroud et al., 2008) and (2) much higher monoterpene yields. Because monoterpene emissions increase exponentially with temperature (Guenther et al., 1991), it is likely that the high temperatures are the driving force of the biogenic event. Although other high-temperature periods occur during the study, they do not result in observations of high biogenic SOA concentrations at Egbert because the air arrives from the south, having passed through the Toronto region. This hampers the isolation of biogenic SOA influence because (1) the Toronto

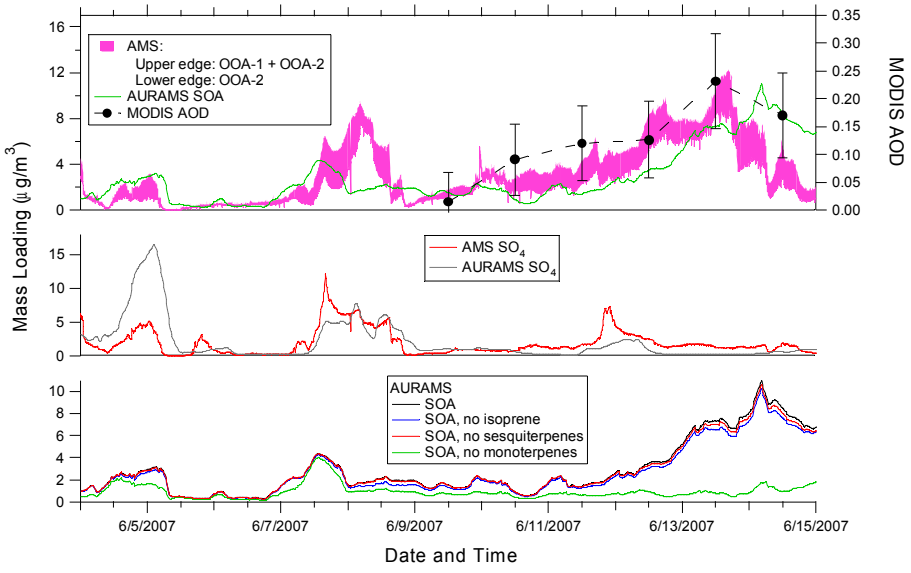

Fig. 9. Comparison of experimental measurements, AURAMS model results, and MODIS regional AOD (top 2 panels), and AURAMS sensitivity tests (bottom panel). AURAMS results are obtained from a 42 km grid in the top and bottom panels and a 15 km grid in the middle panel. Error bars for MODIS AOD denote uncertainties in the retrieval.

outflow contains high concentrations of anthropogenic SOA; and (2) biogenic VOC emissions south of Egbert are dominated by isoprene (rather than monoterpenes) due to the distribution of plant species. The isoprene-dominated emissions decrease the SOA yield and provide a potential OH scavenger (Kiendler-Scharr et al., 2009).

3.4.3 Evaluation of potential biomass burning Influences on the biogenic event

A crucial consideration for the biogenic SOA event discussed here is the extent to which influences from fresh or aged biomass burning aerosol can be ruled out. For clarity, we present elements of the above analysis specifically pertaining to biomass burning influences within this section. For this analysis, we distinguish between the influences of (1) fresh biomass burning and (2) aged biomass burning and discuss the two separately below.

For this discussion, "fresh" biomass burning is defined as the biomass burning contribution to OOA-2, which is identified as fresh by its correlation with MACR+MVK. The following observations suggest that the biomass burning influence is negligible during the biogenic case study:

1. Chemical markers of primary biomass burning emissions (potassium, acetonitrile, BBOA) are negligible (see Fig. 4). Indeed, the onset of the biogenic period is marked by a dramatic reduction in the concentrations of potassium and acetonitrile, contrary to what would occur if a biomass burning period were starting.

2. The $\Delta OM/\Delta CO$ ratio for biogenics is significantly larger than observed in this study or reported in the literature (see Fig. 5a). Further, the difference is also pronounced in the $\Delta OOA\text{-}2/\Delta CO$ ratio.

3. AURAMS accurately predicts SOA concentrations using biogenic (primarily monoterpene) emissions as precursors (see Fig. 9). No biomass burning contribution is required.

4. Analysis of MODIS fire counts (Fig. 10a) and HYSPLIT back trajectories (Fig. 10c) indicate negligible fire influence within half a day of the site. (It is estimated that the OOA-2 must be produced within half a day based on its correlations with MACR+MVK. This is also supported by AURAMS.)

Similar to the preceding discussion, "aged" biomass burning is here defined as the biomass burning contribution to OOA-1. While the source(s) of OOA-1 are more ambiguous than those of OOA-2, the following observations suggest that OOA-1 cannot be attributed to aged biomass burning emissions:

1. Chemical markers of primary biomass burning emissions (potassium, acetonitrile, BBOA) are negligible (see Fig. 4). Acetonitrile and potassium are relatively long-lived. (The atmospheric lifetime of acetonitrile is on the order of several months or longer, see for example (Hamm and Warneck, 1990; Singh. et al., 2003). The lifetime of potassium is the same as that of the particle, which may vary considerably depending on transport and atmospheric processing, but is expected to be

on the order of days to weeks.) The lifetime of BBOA is less certain, although the signal at the characteristic *m/z* 60 and 73 fragments has been observed to disappear as a biomass burrning plume evolves over thousands of kilometers (Capes et al., 2008).

2. Best agreement with AURAMS SOA predictions is obtained through comparison with OOA-1 + OOA-2 (rather than OOA-2 alone), and AURAMS SOA precursors are dominated by monoterpenes (see Fig. 9). Here the OOA-1/OOA-2 analysis and AURAMS represent two independent methods of estimating the biogenic SOA concentration. Comparison between the two methods provides a consistency check for both.

3. Analysis of MODIS fire counts (Fig. 10a) and HYSPLIT 48-h back trajectories (Fig. 10c) are inconsistent with a long-range fire source. Although the trajectories during the final two days of the biogenic period pass near a fire-influenced area, the fires do not begin until after the airmass has passed through. Further, these fires are close enough that significant enhancements in chemical markers of biomass burning would be expected, which as discussed in point (1) does not occur. Finally, the fire counts to the northeast of the site in Fig. 10a represent the only major fires in Canada during the biogenic period.

4. As shown in Fig. 10c, the trajectories during the biogenic period originate from a variety of locations north of Egbert. Given that biomass burning emissions are expected to be localized (e.g. Fig. 10a), the combination of a the observed $\Delta OM/\Delta CO$ ratio and tight correlation between organic mass and CO is not consistent with biomass burning origins. While a photochemical age-independent $\Delta OM/\Delta CO$ has been previously observed (Capes et al., 2008), Table 1 shows that the $\Delta OM/\Delta CO$ during the biogenic period is at least a factor of 2 higher than for fresh biomass burning emissions and higher than all previously reported values in aged biomass burning studies. An $\Delta OM/\Delta CO$ ratio that increases with atmospheric processing due to SOA production is required to obtain such a high value. A tight OM/CO correlation will not occur under such conditions, as CO is dominated by primary emissions. However, the combination of high $\Delta OM/\Delta CO$ and tight OM/CO correlation is in fact observed (see Fig. 5) and is consistent with photochemically-generated CO from a widespread biogenic source from forested regions.

3.5 Regional Impact of Biogenic SOA

Remote sensing measurements suggest that the high levels of particulate organics observed in this study are representative of the regional contribution of biogenic VOC emissions.

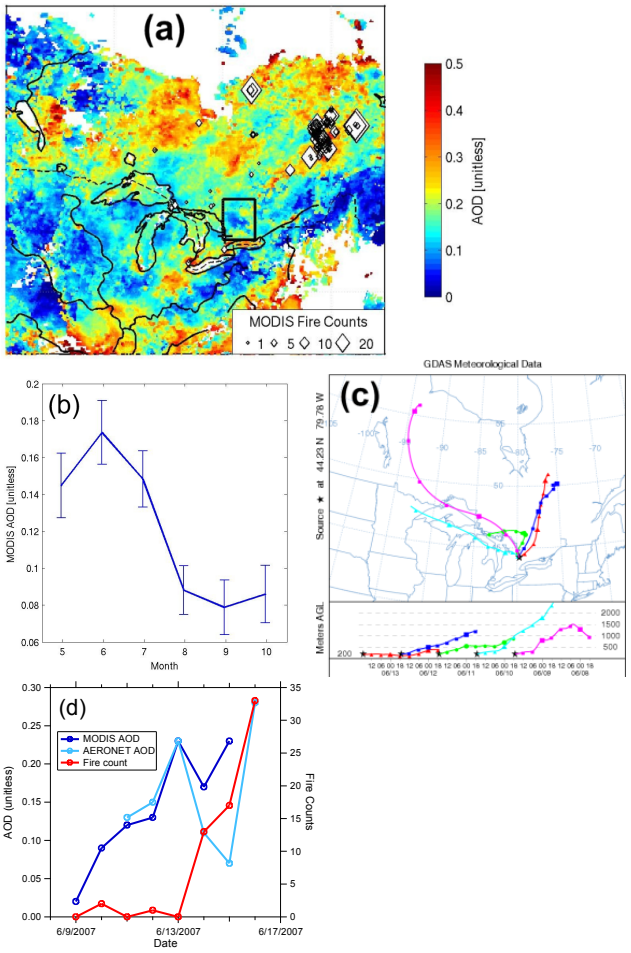

Fig. 10. **(a)** MODIS aerosol optical depth (colors) and fire counts (diamonds) over Ontario and Quebec during the peak of the biogenic period (12 to 14 June 2007). The sampling location is denoted as a cross; the 3° by 3° box was used to calculate regional AOD in Fig. 9. **(b)** Monthly MODIS AOD average from 2001 to 2006 calculated within the boxed region of Fig. 10a. Error bars denote uncertainties in the MODIS AOD retrieval. **(c)** 48-h back trajectories ending at the Egbert site. **(d)** MODIS AOD from the boxed region in Fig. 10a, AERONET AOD at the Egbert site, and MODIS fire counts over the entire region of Fig. 10a. Fire counts are negligible until 14 June, at which point the wind abruptly shifts from north to south, preventing fire emissions from reaching the site.

This is shown in Fig. 9 by the correlated increases of observed and modeled biogenic SOA with the regional AOD, retrieved from the MODIS satellite instrument (Salomonson et al., 1989) for the box defined by 44° to 47° N and 77° to 80° W, containing Egbert in its southwest corner. Figure 10a shows the AOD over northern Ontario and Quebec during the biogenic period (9 to 13 June), with the locations of Egbert and the previously described box displayed. A widespread region of elevated AOD exists over the sparsely populated, boreal forest region to the north of the sampling location. This region corresponds approximately with the region of

high biogenic SOA predicted by AURAMS (see Fig. 7). MODIS fire counts to the north are negligible, though some fires were observed in regions to the northeast. Back trajectories (48-h duration) from the Egbert site are shown in Fig. 10c. Contamination from the single fire count detected to the southwest is unlikely given its short duration (a single day), prevailing northerly winds, and measured aerosol composition. Figure 10d shows MODIS AOD for the boxed region of Fig. 10a, AERONET AOD at the Egbert site, and MODIS fire counts over the entire region of Fig. 10a for the period 9 to 16 June. Fire counts are negligible until 14 June. However, at this point, the wind abruptly shifts from north to south and Egbert samples the Toronto urban outflow; the fire emissions never reach the site.

Figure 10b shows the monthly averages of AOD from 2001 to 2006 for the boxed region, suggesting that this biogenic radiative forcing effect is strongest in the late spring and early summer, although biomass burning emissions have also affected the site during this period (e.g. June and July of 2004 (Pfister et al., 2005; McMillan et al., 2008). A similar seasonal cycle has been observed in the southeast United States (Goldstein et al., 2009), where isoprene is the dominant biogenic VOC. Egbert mean AOD during summer is typically lower than that reported by Goldstein et al. ($\sim$0.16 vs. $\sim$0.35). The lower values at Egbert are probably due to (1) lower temperatures (resulting in lower monoterpene emissions, which increase exponentially with temperature), and (2) decreased anthropogenic influence. However, Egbert AOD climbed to 0.23 during the biogenic event, with significantly higher values ($\sim$0.4) farther north (see Fig. 10a). The seasonal cycle shown in Fig. 10b shows significantly lower AOD in August, despite the expectation of similar temperatures, indicating that factors other than temperature (e.g. meteorology, biological factors) also influence the regional AOD. The identity and importance of such factors is uncertain and would would be an interesting issue for future study.

The increased AOD will have a significant regional cooling effect in clear-sky conditions over a (relatively dark) forest, while a smaller warming effect will be produced from the CO_2 generated from the photochemically-produced biogenic CO. Further cooling will result from the cloud condensation nuclei activity of the biogenic SOA, which reached a maximum value of $\sim$1600 cm^{-3} during the biogenic period (0.42% supersaturation) vs. $\sim$3000 cm^{-3} during the 30 May to 3 June urban outflow period. The high particle concentration and CCN activity are consistent with a significant climate cooling effect from biogenic aerosol arising from mid-latitude forests, as suggested by a recent modeling study (Spracklen et al., 2008).

4 Conclusions

Organic concentrations reaching levels $\sim$5 times higher than most previous measurements for biogenic aerosols are observed, likely resulting from monoterpene emissions from Canadian coniferous forests driven by elevated temperatures. Biogenic OM is identified from correlations with tracer VOCs and by the relationship of the total OM and oxygenated components with CO. The observations provide evidence for a significant photochemical source of biogenic CO. Biogenic SOA concentrations are accurately predicted by a regional air quality model, in contrast to model underpredictions reported in more polluted regions. Model calculations and remote sensing measurements indicate that the high mass loading is widespread, implying that biogenic SOA contributes strongly to the regional aerosol, presumably in both rural and urban locations in Southern Ontario. The high particle concentration and CCN activity are consistent with a significant climate cooling effect from biogenic aerosol arising from mid-latitude forests.

Acknowledgements. This work was supported by the Canadian Foundation for Climate and Atmospheric Sciences through the Cloud-Aerosol Feedbacks and Climate Network and by the Natural Science and Engineering Research Council (Canada). Partial infrastructure funding came from CFI and OIT. The authors also thank Dr. Jiannan Li for discussion of the radiative forcing calculations, Prof. Rainer Volkamer for discussion of the SOA yield calculation, and the MODIS team for measurements of aerosol optical depth.

Edited by: J.-L. Jimenez

References

Aiken, A. C., DeCarlo, P. F., Kroll, J. H., Worsnop, D. R., Huffman, J. A., Docherty, K. S., Ulbrich, I. M., Mohr, C., Kimmel, J. R., Sueper, D., Sun, Y., Zhang, Q., Trimborn, A., Northway, M., Ziemann, P. J., Canagaratna, M. R., Onasch, T. B., Alfarra, M. R., Prevot, A. S. H., Dommen, J., Duplissy, J., Metzger, A., Baltensperger, U., and Jimenez, J. L.: O/C and OM/OC Ratios of Primary, Secondary, and Ambient Organic Aerosols with High-Resolution Time-of-Flight Aerosol Mass Spectrometry, Environ. Sci. Technol., 42, 4478–4485, doi:10.1021/es703009q, 2008.

Aiken, A. C., Salcedo, D., Cubison, M. J., Huffman, J. A., DeCarlo, P. F., Ulbrich, I. M., Docherty, K. S., Sueper, D., Kimmel, J. R., Worsnop, D. R., Trimborn, A., Northway, M., Stone, E. A., Schauer, J. J., Volkamer, R. M., Fortner, E., de Foy, B., Wang, J., Laskin, A., Shutthanandan, V., Zheng, J., Zhang, R., Gaffney, J., Marley, N. A., Paredes-Miranda, G., Arnott, W. P., Molina, L. T., Sosa, G., and Jimenez, J. L.: Mexico City aerosol analysis during MILAGRO using high resolution aerosol mass spectrometry at the urban supersite (T0) - Part 1: Fine particle composition and organic source apportionment, Atmos. Chem. Phys., 9, 6633–6653, 2009,
http://www.atmos-chem-phys.net/9/6633/2009/.

Allan, J. D., Jimenez, J. L., Williams, P. I., Alfarra, M. R., Bower, K. N., Jayne, J. T., Coe, H., and Worsnop, D. R.: Quantitative sampling using an Aerodyne aerosol mass spectrometer 1: Techniques of data interpretation and error analysis, J. Geophys. Res., 108, 4090: doi:10.1029/2002JD002358, 2003.

Biesenthal, T. A., Bottenheim, J. W., Shepson, P. B., Li, S.-M., and Brickell, P. C.: The chemistry of biogenic hydrocarbons at a rural site in eastern Canada, J. Geophys. Res., 103, 25487–25498, 1998.

Brickell, P. C., Bottenheim, J. W., Froude, F., and Jiang, Z.: In-Situ NMHC Measurements in Rural Ontario, Canada, Eos. Trans. AGU, Fall Meeting, A31D-0070, 2003.

Canagaratna, M. R., Jayne, J. T., Jimenez, J. L., Allan, J. D., Alfarra, M. R., Zhang, Q., Onasch, T. B., Drewnick, F., Coe, H., Middlebrook, A. M., Delia, A., Williams, L. R., Trimborn, A. M., Northway, M. J., DeCarlo, P. F., Kolb, C. E., Davidovits, P., and Worsnop, D. R.: Chemical and microphysical characterization of ambient aerosols with the Aerodyne aerosol mass spectrometer, Mass Spec. Rev., 26, 185–222, 2007.

Capes, G., Johnson, B., McFiggans, G., Williams, P. I., Haywood, J., and Coe, H.: Aging of biomass burning aerosols over West Africa: Aircraft measurements of chemical composition, microphysical properties, and emission ratios, J. Geophys. Res., 113, D00C15, doi:10.1029/2008JD009845, 2008.

Capes, G., Murphy, J. G., Reeves, C. E., McQuaid, J. B., Hamilton, J. F., Hopkins, J. R., Crosier, J., Williams, P. I., and Coe, H.: Secondary organic aerosol from biogenic VOCs over West Africa during AMMA, Atmos. Chem. Phys., 9, 3841–3850, 2009, http://www.atmos-chem-phys.net/9/3841/2009/.

CEP, Carolina Environmental Program, Sparse Matrix Operator Kernel 1 Emission (SMOKE) modelling system, pp. see http://www.smoke-model.org/index.cfm, University of North Carolina, Carolina Environmental Programs, Chapel Hill, NC, 2003.

Chang, R. Y.-W., Liu, P. S. K., Leaitch, W. R., and Abbatt, J. P. D.: Comparison between measured and predicted CCN concentrations at Egbert, Ontario: Focus on the organic aerosol fraction at a semi-rural site, Atmos. Environ., 41, 8172–8182, 2007.

Chang, R. Y.-W., Slowik, J. G., Shantz, N. C., Vlasenko, A., Liggio, J., Sjostedt, S. J., Leaitch, W. R., and Abbatt, J. P. D.: The hygroscopicity parameter (?) of ambient organic aerosol at a field site subject to biogenic and anthropogenic influences: Relationship to degree of aerosol oxidation, Atmos. Chem. Phys. Discuss., 9, 25323–25360, 2009, http://www.atmos-chem-phys-discuss.net/9/25323/2009/.

Chen, Q., Farmer, D. K., Schneider, J., Zorn, S. R., Heald, C. L., Karl, T. G., Guenther, A., Allan, J. D., Robinson, N., Coe, H., Kimmel, J. R., Pauliquevis, T., Borrmann, S., Poschl, U., Andreae, M. O., Artaxo, P., Jimenez, J. L., and Martin, S. T.: Mass spectral characterization of submicron biogenic organic particles in the Amazon Basin, Geophys. Res. Let., 36, L20806, doi:10.1029/2009GL039880, 2009.

Claeys, M., Braham, B., Vas, G., Wang, W., Vermeylen, R., Pashynska, V., Cafmeyer, J., Guyon, P., Andreae, M. O., Artaxo, P., and Maenhaut, W.: Formation of Secondary Organic Aerosols Through Photooxidation of Isoprene, Science, 303, 1173–1176, 2004.

Côté, J., Desmarais, J.-G., Gravel, S., Méthot, A., Patoine, A., Roch, M., and Staniforth, A.: The operational CMC-MRB global environmental multiscale (GEM) model. Part I: Design considerations and formulation, Mon. Weather Rev., 126, 1373–1395, 1998a.

Côté, J., Desmarais, J.-G., Gravel, S., Méthot, A., Patoine, A., Roch, M., and Staniforth, A.: The operational CMC-MRB global environmental multiscale (GEM) model. Part II: Results, Mon. Weather Rev., 126, 1397–1418, 1998b.

Cross, E. S., Onasch, T. B., Canagaratna, M., Jayne, J. T., Kimmel, J., Yu, X.-Y., Alexander, M. L., Worsnop, D. R., and Davidovits, P.: Single particle characterization using a light scattering module coupled to a time-of-flight aerosol mass spectrometer, Atmos. Chem. Phys., 9, 7769–7793, 2009, http://www.atmos-chem-phys.net/9/7769/2009/.

Cross, E. S., Slowik, J. G., Davidovits, P., Allan, J. D., Worsnop, D. R., Jayne, J. T., Lewis, D. K., Canagaratna, M. R., and Onasch, T. B.: Laboratory and Ambient Particle Density Determinations using Light Scattering in Conjunction with Aerosol Mass Spectrometry, Aerosol Sci. Technol., 41, 343–359, doi:10.1080/02786820701199736, 2007.

de Gouw, J. A., Brock, C. A., Atlas, E. L., Bates, T. S., Fehsenfeld, F. C., Goldan, P. D., Holloway, J. S., Kuster, W. C., Lerner, B. M., Matthew, B. M., Middlebrook, A. M., Onasch, T. B., Peltier, R. E., Quinn, P. K., Senff, C. J., Stohl, A., Sullivan, A. P., Trainer, M., Warneke, C., Weber, R. L., and Williams, E. J.: Sources of particulate matter in the northeastern United States in summer: 1. Direct emissions and secondary formation of organic matter in urban plumes, J. Geophys. Res., 113, D08301, doi:10.1029/2007JD009243, 2008.

de Gouw, J. A. and Warneke, C.: Measurements of volatile organic compounds in the Earth's atmosphere using proton-transfer-reaction mass spectrometry, Mass Spec. Rev., 26, 223–257, 2007.

DeCarlo, P. F., Dunlea, E. J., Kimmel, J. R., Aiken, A. C., Sueper, D., Crounse, J., Wennberg, P. O., Emmons, L., Shinozuka, Y., Clarke, A., Zhou, J., Tomlinson, J., Collins, D. R., Knapp, D., Weinheimer, A. J., Montzka, D. D., Campos, T., and Jimenez, J. L.: Fast airborne aerosol size and chemistry measurements above Mexico City and Central Mexico during the MILAGRO campaign, Atmos. Chem. Phys., 8, 4027–4048, 2008, http://www.atmos-chem-phys.net/8/4027/2008/.

DeCarlo, P. F., Kimmel, J. R., Trimborn, A., Northway, M. J., Jayne, 1 J. T., Aiken, A. C., Gonin, M., Fuhrer, K., Horvath, T., Docherty, K. S., Worsnop, D. R., and Jimenez, J. L.: Field-Deployable, High-Resolution, Time-of-Flight Aerosol Mass Spectrometer, Anal. Chem., 78, 8281–8289, 2006.

Drewnick, F., Hings, S. S., Curtius, J., Eerdekens, G., and Williams, J.: Measurement of fine particulate and gas-phase species during the New Year's fireworks 2005 in Mainz, Germany, Atmos. Environ., 40, 4316–4327, 2006.

Drewnick, F., Hings, S. S., DeCarlo, P. F., Jayne, J. T., Gonin, M., Fuhrer, K., Weimer, S., Jimenez, J. L., Demerjian, K. L., Borrmann, S., and Worsnop, D. R.: A new Time-of-Flight Aerosol Mass Spectrometer (ToF-AMS) – Instrument description and first field deployment, Aerosol Sci. Technol., 39, 637–658, 2005.

Dzepina, K., Volkamer, R. M., Madronich, S., Tulet, P., Ulbrich, I. M., Zhang, Q., Cappa, C. D., Ziemann, P. J., and Jimenez, J. L.: Evaluation of recently-proposed secondary organic aerosol models for a case study in Mexico City, Atmos. Chem. Phys., 9, 5681–5709, 2009, http://www.atmos-chem-phys.net/9/5681/2009/.

Giglio, L., Descloitres, J., Justice, C. O., and Kaufman, Y. J.: An Enhanced Contextual Fire Detection Algorithm for MODIS, Remote Sens. Environ., 87, 273–282, 2003.

Goldstein, A. H. and Galbally, I. E.: Known and Unexplored Organic Constituents in the Earth's Atmosphere, Environ. Sci. Technol., 41, 1514–1521, 2007.

Goldstein, A. H., Koven, C. D., Heald, C. L., and Fung, I. Y.: Biogenic carbon and anthropogenic pollutants combine to form a cooling haze over the southeastern United States, Proc. Nat. Acad. Sci., 106, 8835–8840, doi:10.1073/pnas.0904128106, 2009.

Gong, S. L., Barrie, L. A., Blanchet, J.-P., von Salzen, K., Lohmann, U., Lesins, G., Spacek, L., Zhang, L. M., Girard, E., Lin, H., Leaitch, W. R., Leighton, H., Chylek, P., and Huang, P.: Canadian Aerosol Module: A size-segregated simulation of atmospheric aerosol processes for climate and air quality models. 1. Module development, J. Geophys. Res. D: Atmospheres, 108, AAC 3-1 AAC 3-16, 2003.

Grieshop, A. P., Logue, J. M., Donahue, N. M., and Robinson, A. L.: Laboratory investigation of photochemical oxidation of organic aerosol from wood fires 1: measurement and simulation of organic aerosol evolution, Atmos. Chem. Phys., 9, 1263–1277, 2009, http://www.atmos-chem-phys.net/9/1263/2009/.

Grieshop, A. P., Donahue, N. M., and Robinson, A. L.: Laboratory investigation of photochemical oxidation of organic aerosol from wood fires 2: analysis of aerosol mass spectrometer data, Atmos. Chem. Phys., 9, 2227–2240, 2009, http://www.atmos-chem-phys.net/9/2227/2009/.

Griffin, R. J., Cocker III, D. R., Flagan, R. C., and Seinfeld, J. H.: Organic aerosol formation from the oxidation of biogenic hydrocarbons, J. Geophys. Res.-Atmos., 104, 3555–3567, 1999.

Guenther, A., Geron, C., Pierce, T., Lamb, B., Harley, P., and Fall, R.: Natural emissions of non-methane volatile organic compounds, carbon monoxide, and oxides of nitrogen from North America, Atmos. Environ., 34, 2205–2230, 2000.

Guenther, A., Otter, L., Zimmerman, P., Greenberg, J., Scholes, R., and Scholes, M.: Biogenic hydrocarbon emissions from southern African savannas, J. Geophys. Res., 101, 25859–25865, 1996.

Guenther, A. B., Monson, R. K., and Fall, R.: Isoprene and Monoterpene Emission Rate Variability: Observations With Eucalyptus and Emission Rate Algorithm Development, J. Geophys. Res., 96, 10799–10808, 1991.

Gunthe, S. S., King, S. M., Rose, D., Chen, Q., Roldin, P., Farmer, D. K., Jimenez, J. L., Artaxo, P., Andreae, M. O., Martin, S. T., and Pöschl, U.: Cloud condensation nuclei in pristine tropical rainforest air of Amazonia: size-resolved measurements and modeling of atmospheric aerosol composition and CCN activity, Atmos. Chem. Phys., 9, 7551–7575, 2009, http://www.atmos-chem-phys.net/9/7551/2009/.

Hallquist, M., Wenger, J. C., Baltensperger, U., Rudich, Y., Simpson, D., Claeys, M., Dommen, J., Donahue, N. M., George, C., Goldstein, A. H., Hamilton, J. F., Herrmann, H., Hoffmann, T., Iinuma, Y., Jang, M., Jenkin, M. E., Jimenez, J. L., Kiendler-Scharr, A., Maenhaut, W., McFiggans, G., Mentel, Th. F., Monod, A., Prévôt, A. S. H., Seinfeld, J. H., Surratt, J. D., Szmigielski, R., and Wildt, J.: The formation, properties and impact of secondary organic aerosol: current and emerging issues, Atmos. Chem. Phys., 9, 5155–5236, 2009, http://www.atmos-chem-phys.net/9/5155/2009/.

Hamm, S. and Warneck, P.: The interhemispheric distribution and the budget of acetonitrile in the troposphere, J. Geophys. Res.-Atmos., 95, 20593–20606, 1990.

Helmig, D., Ortega, J., Duhl, T., Tanner, D., Guenther, A., Harley, P., Wiedinmyer, C., Milford, J., and Sakulyanontvittaya, T.: Sesquiterpene emissions from pine trees – identifications, emission rates and flux estimates for the contiguous United States, Environ. Sci. Technol., 41, 1545–1553, 2007.

Henze, D. K., Seinfeld, J. H., Ng, N. L., Kroll, J. H., Fu, T.-M., Jacob, D. J., and Heald, C. L.: Global modeling of secondary organic aerosol formation from aromatic hydrocarbons: high-vs. low-yield pathways, Atmos. Chem. Phys., 8, 2405–2420, 2008, http://www.atmos-chem-phys.net/8/2405/2008/.

Hildebrandt, L., Donahue, N. M., and Pandis, S. N.: High formation of secondary organic aerosol from the photo-oxidation of toluene, Atmos. Chem. Phys., 9, 2973–2986, 2009, http://www.atmos-chem-phys.net/9/2973/2009/.

Holben, B. N., Tanre, D., Smirnov, A., Eck, T. F., Slutsker, I., Abuhassan, N., Newcomb, W. W., Schafer, J. S., Chatenet, B., Lavenu, F., Kaufman, Y. J., Vande Castle, J., Setzer, A., Markham, B., Clark, D., Frouin, R., Halthore, R., Karneli, A., O'Neill, N. T., Pietras, C., Pinker, R. T., Voss, K., and Zibordi, G.: An emerging ground-based aerosol climatology: Aerosol optical depth from AERONET, J. Geophys. Res., 106, 12067–12097, 2001.

Houyoux, M. R., Vukovich, J. M., Coats, C. J. J., and Wheeler, N. J. M.: Emission inventory development and processing for the Season Model for Regional Air Quality (SMRAQ) project, J. Geophys. Res., 105, 9079–9090, 2000.

Hudman, R. C., Murray, L. T., Jacob, D. J., Millet, D. B., Turquety, S., Wu, S., Blake, D. R., Goldstein, A. H., Holloway, J., and Sachse, G. W.: Biogenic versus anthropogenic sources of CO in the United States, Geophys. Res. Let., 35, L04801, doi:10.1029/2007GL032393, 2008.

Huffman, J. A., Docherty, K. S., Aiken, A. C., Cubison, M. J., Ulbrich, I. M., DeCarlo, P. F., Sueper, D., Jayne, J. T., Worsnop, D. R., Ziemann, P. J., and Jimenez, J. L.: Chemically-resolved aerosol volatility measurements from two megacity field studies, Atmos. Chem. Phys., 9, 7161–7182, 2009, http://www.atmos-chem-phys.net/9/7161/2009/.

Jayne, J. T., Leard, D. C., Zhang, X. F., Davidovits, P., Smith, K. A., Kolb, C. E., and Worsnop, D. R.: Development of an Aerosol Mass Spectrometer for Size and Composition Analysis of Submicron Particles, Aerosol Sci. Technol., 33, 49–70, 2000.

Jimenez, J. L., Canagaratna, M. R., Donahue, N. M., Prevot, A. S. H., Zhang, Q., Kroll, J. H., DeCarlo, P. F., Allan, J. D., Coe, H., Ng, N. L., Aiken, A. C., Docherty, K. D., Ulbrich, I. M., Grieshop, A. P., Robinson, A. L., Duplissy, J., Smith, J. D., Wilson, K. R., Lanz, V. A., Hueglin, C., Sun, Y. L., Tian, J., Laaksonen, A., Raatikainen, T., Rautiainen, J., Vaattovaara, P., Ehn, M., Kulmala, M., Tomlinson, J. M., Collins, D. R., Cubison, M. J., Dunlea, E. J., Huffman, J. A., Onasch, T. B., Alfarra, M. R., Williams, P. I., Bower, K., Kondo, Y., Schneider, J., Drewnick, F., Borrmann, S., Weimer, S., Demerjian, K. L., Salcedo, D., Cottrell, L., Griffin, R. J., Takami, A., Miyoshi, T., Hatakeyama, S., Shimono, A., Sun, J. Y., Zhang, Y. M., Dzepina, K., Kimmel, J. R., Sueper, D., Jayne, J. T., Herndon, S. C., Trimborn, A. M.,

Williams, L. R., 1 Wood, E. C., Kolb, C. E., Middlebrook, A. M., Baltensperger, U., and Worsnop, D.R.: Evolution of organic aerosols in the atmosphere, Science, 326, 1525–1529, 2009.

Jimenez, J. L., Jayne, J. T., Shi, Q., Kolb, C. E., Worsnop, D. R., Yourshaw, I., Seinfeld, J. H., Flagan, R. C., Zhang, X. F., Smith, K. A., Morris, J. W., and Davidovits, P.: Ambient Aerosol Sampling with an Aerosol Mass Spectrometer, J. Geophys. Res., 108, 8425, doi:8410:1029/2001JD001213, 2003.

Johnson, D., Utembe, S. R., Jenkin, M. E., Derwent, R. G., Hayman, G. D., Alfarra, M. R., Coe, H., and McFiggans, G.: Simulating regional scale secondary organic aerosol formation during the TORCH 2003 campaign in the southern UK, Atmos. Chem. Phys., 6, 403–418, 2006, http://www.atmos-chem-phys.net/6/403/2006/.

Kanakidou, M., Seinfeld, J. H., Pandis, S. N., Barnes, I., Dentener, F. J., Facchini, M. C., Van Dingenen, R., Ervens, B., Nenes, A., Nielsen, C. J., Swietlicki, E., Putaud, J. P., Balkanski, Y., Fuzzi, S., Horth, J., Moortgat, G. K., Winterhalter, R., Myhre, C. E. L., Tsigaridis, K., Vignati, E., Stephanou, E. G., and Wilson, J.: Organic aerosol and global climate modelling: a review, Atmos. Chem. Phys., 5, 1053–1123, 2005, http://www.atmos-chem-phys.net/5/1053/2005/.

Kavouras, I. G., Mihalopoulos, M., and Stephanou, E. G.: Formation of atmospheric particles from organic acids produced by forests, Nature, 395, 683–686, 1998.

Kiendler-Scharr, A., Wildt, J., Dal Maso, M., Hohaus, T., Kleist, E., Mentel, T. F., Tillmann, R., Uerlings, R., Schurr, U., and Wahner, A.: New particle formation in forests inhibited by isoprene emissions, Nature, 461, 381–384, 2009.

Kleinman, L. I., Springston, S. R., Wang, J., Daum, P. H., Lee, Y.-N., Nunnermacker, L. J., Senum, G. I., Weinstein-Lloyd, J., Alexander, M. L., Hubbe, J., Ortega, J., Zaveri, R. A., Canagaratna, M. R., and Jayne, J.: The time evolution of aerosol size distribution over the Mexico City plateau, Atmos. Chem. Phys., 9, 4261–4278, 2009, http://www.atmos-chem-phys.net/9/4261/2009/.

Kroll, J. H., Ng, N. L., Murphy, S. M., Flagan, R. C., and Seinfeld, J. H.: Secondary aerosol formation from isoprene photooxidaation, Environ. Sci. Technol., 40, 1869–1877, 2006.

Kuhn, M., Builtjes, P. J. H., Poppe, D., Simpson, D., Stockwell, W. R., Andersson-Sköld, Y., Baart, A., Das, M., Fiedler, F., Hov, Ø., Kirchner, F., Makar, P. A., Milford, J. B., Roemer, M. G. M., Ruhnke, R., Strand, A., Vogel, B., and Vogel, H.: Intercomparison of the gas-phase chemistry in several chemistry and transport models, Atmos. Environ., 32, 693–709, 1998.

Pradeep Kumar, P., Broekhuizen, K., and Abbatt, J. P. D.: Organic acids as cloud condensation nuclei: Laboratory studies of highly soluble and insoluble species, Atmos. Chem. Phys., 3, 509–520, 2003, http://www.atmos-chem-phys.net/3/509/2003/.

Lane, T. E., Donahue, N. M., and Pandis, S. N.: Effect of NOx on secondary organic aerosol concentrations, Environ. Sci. Technol., 42, 6022–6027, 2008.

Lanz, V. A., Alfarra, M. R., Baltensperger, U., Buchmann, B., Hueglin, C., and Prévôt, A. S. H.: Source apportionment of submicron organic aerosols at an urban site by factor analytical modelling of aerosol mass spectra, Atmos. Chem. Phys., 7, 1503–1522, 2007, http://www.atmos-chem-phys.net/7/1503/2007/.

Lanz, V. A., Alfarra, M. R., Baltensperger, U., Buchmann, B., Hueglin, C., Szidat, S., Wehrli, M. N., Wacker, L., Weimer, S., Caseiro, A., Puxbaum, H., and Prévôt, A. S. H.: Source Attribution of Submicron Organic Aerosols during Wintertime Inversions by Advanced Factor Analysis of Aerosol Mass Spectra, Environ. Sci. Technol., 42, 214–220, 2008.

Lee, A., Goldstein, A. H., Keywood, M. D., Gao, S., Varutbangkul, V., Bahreini, R., Ng, N. L., Flagan, R. C., and Seinfeld, J. H.: Gas-phase products and secondary aerosol yields from the ozonolysis of ten different terpenes, J. Geophys. Res., 111, D07302, doi:10.1029/2005JD006437, 2006a.

Lee, A., Goldstein, A. H., Kroll, J. H., Ng, N. L., Varutbangkul, V., Flagan, R. C., and Seinfeld, J. H.: Gas-phase products and secondary aerosol yields from the photooxidation of 16 different terpenes, J. Geophys. Res., 111, D17305, doi:10.1029/2006JD007050, 2006b.

Levy, R. C., Remer, L. A., Mattoo, S., Vermote, E. F., and Kaufman, Y. J.: Second-generation operational algorithm: Retrieval of aerosol properties over land from inversion of Moderate Resolution Imaging Spectroradiometer Spectral reflectance, J. Geophys. Res., 112, D13211, doi:10.1029/2006JD007811, 2007.

Lindinger, W., Hansel, A., and Jordan, A.: Proton-transfer reaction mass spectrometry (PTR-MS): on-line monitoring of volatile organic compounds at pptv levels, Chem. Soc. Rev., 27, 347–354, 1998.

Matthew, B. M., Middlebrook, A. M., and Onasch, T. B.: Collection Efficiencies in an Aerodyne Aerosol Mass Spectrometer as a Function of Particle Phase for Laboratory Generated Aerosols, Aerosol Sci. Technol., 42, 884–898, 2008.

McMillan, W. W., Warner, J. X., McCourt Comer, M., Maddy, E., Chu, A., Sparling, L., Eloranta, E., Hoff, R., Sachse, G., Barnet, C., Razenkov, I., and Wolf, W.: AIRS views transport from 12 to 22 July 2004 Alaskan/Canadian fires: Correlation of AIRS CO and MODIS AOD with forward trajectories and comparison of AIRS CO retrievals with DC-8 in situ measurements during INTEX-A/ICARTT, J. Geophys. Res., 113, D20301, doi:10.1029/2007JD009711, 2008.

Miller, S. M., Matross, D. M., Andrews, A. E., Millet, D. B., Longo, M., Gottlieb, E. W., Hirsch, A. I., Gerbig, C., Lin, J. C., Daube, B. C., Hudman, R. C., Dias, P. L. S., Chow, V. Y., and Wofsy, S. C.: Sources of carbon monoxide and formaldehyde in North America determined from high-resolution atmospheric data, Atmos. Chem. Phys., 8, 7673–7696, 2008, http://www.atmos-chem-phys.net/8/7673/2008/.

Moran, M. D., Dastoor, A., Gong, S. L., Gong, W., and Makar, P. A., Proposed Conceptual Design for the AES Regional Particulate Matter Model/Unified Model, pp. 100 pp [Available from first author], Meteorological Service of Canada, Downsview, ON, Canada, 1998.

Ng, N. L., Chhabra, P. S., Chan, A. W. H., Surratt, J. D., Kroll, J. H., Kwan, A. J., McCabe, D. C., Wennberg, P. O., Sorooshian, A., Murphy, S. M., Dalleska, N. F., Flagan, R. C., and Seinfeld, J. H.: Effect of NOx level on secondary organic aerosol (SOA) formation from the photooxidation of terpenes, Atmos. Chem. Phys., 7, 5159–5174, 2007, http://www.atmos-chem-phys.net/7/5159/2007/.

Ng, N. L., Kroll, J. H., Chan, A. W. H., Chhabra, P. S., Flagan, R. C., and Seinfeld, J. H.: Secondary organic aerosol formation from *m*-xylene, toluene, and benzene, Atmos. Chem. Phys., 7,

3909–3922, 2007,
http://www.atmos-chem-phys.net/7/3909/2007/.

Odum, J. R., Hoffman, T., Bowman, F., Collins, D., Flagan, R. C., and Seinfeld, J. H.: Gas/particle partitioning and secondary organic aerosol yields, Environ. Sci. Technol., 8, 2580–2585, 1996.

Paatero, P.: Least squares formulation of robust non-negative factor analysis, Chemom. Intell. Lab. Syst., 37, 23–35, 1997.

Paatero, P. and Tapper, U.: Positive Matrix Factorization: A non-negative factor model with optimal utilization of error estimates of data values, Environmetrics, 5, 111–126, 1994.

Pankow, J. F.: An absorption model of the gas/aerosol partitioning involved in the formation of secondary organic aerosol, Atmos. Environ., 28, 189–193, 1994.

Pathak, R. K., Presto, A. A., Lane, T. E., Stanier, C. O., Donahue, N. M., and Pandis, S. N.: Ozonolysis of α-pinene: parameterization of secondary organic aerosol mass fraction, Atmos. Chem. Phys., 7, 3811–3821, 2007,
http://www.atmos-chem-phys.net/7/3811/2007/.

Pfister, G., Hess, P. G., Emmons, L. K., Lamarque, J.-F., Wiedinmyer, C., Edwards, D. P., Petron, G., Gille, J. C., and Sachse, G. W.: Quantifying CO emissions from the 2004 Alaskan wildfires using MOPITT CO data, Geophys. Res. Let., 32, L11809, doi:10.1029/2005GL022995, 2005.

Presto, A. A. and Donahue, N. M.: Investigation of R-pinene + ozone secondary organic aerosol formation at low total aerosol mass, Environ. Sci. Technol., 40, 3536–3543, 2006.

Rappenglück, B., Apel, E., Bauerfeind, M., Bottenheim, J. W., Brickell, P. C., Cavolka, P., Cech, J., Gatti, L., Hakola, H., Honzak, J., Junek, R., Martin, D., Noone, C., Plass-Dülmer, C., Travers, D., and Wang, D.: The first VOC intercomparison exercise within the Global Atmosphere Watch (GAW), Atmos. Environ., 40, 7508–7527, 2006.

Reid, J. S., Koppmann, R., Eck, T. F., and Eleuterio, D. P.: A review of biomass burning emissions part II: intensive physical properties of biomass burning particles, Atmos. Chem. Phys., 5, 799–825, 2005,
http://www.atmos-chem-phys.net/5/799/2005/.

Remer, L. A., Kaufman, Y. J., Tanre, D., Mattoo, S., Chu, D. A., Martins, J. V., Li, R.-R., Ichoku, C., Levy, R. C., Kleidman, R. G., Eck, T. F., Vermote, E. F., and Holben, B. N.: The MODIS Aerosol Algorithm, Products and Validation, J. Atmos. Sci., Special Section, 62, 947–973, 2005.

Rupakheti, M., Leaitch, W. R., Lohmann, U., Hayden, K. L., Brickell, P., Lu, G., Li, S.-M., Toom-Sauntry, D., Bottenheim, J. W., Brook, J. R., Vet, R., Jayne, J. T., and Worsnop, D. R.: An Intensive Study of the Size and Composition of Submicron Atmospheric Aerosols at a Rural Site in Ontario, Canada, Aerosol Sci. Technol., 39, 722–736, 2005.

Salomonson, V. V., Barnes, W. L., Maymon, P. W., Montgomery, H. E., and Ostrow, H.: MODIS: Advanced Facility Instrument for Studies of the Earth as a System, IEEE Transactions on Geoscience and Remote Sensing, 27, 145–153, 1989.

Sandu, A. and Sander, R.: Technical note: Simulating chemical systems in Fortran90 and Matlab with the Kinetic PreProcessor KPP-2.1, Atmos. Chem. Phys., 6, 187–195, 2006,
http://www.atmos-chem-phys.net/6/187/2006/.

Saunders, S. M., Jenkin, M. E., Derwent, R. G., and Pilling, M. J.: Protocol for the development of the Master Chemical Mechanism, MCM v3 (Part A): tropospheric degradation of non-aromatic volatile organic compounds, Atmos. Chem. Phys., 3, 161–180, 2003,
http://www.atmos-chem-phys.net/3/161/2003/.

Schneider, J., Weimer, S., Drewnick, F., Borrmann, S., Helas, G., Gwaze, P., Schmid, O., Andreae, M. O., and Kirchner, U.: Mass spectrometric analysis and aerodynamic properties of various types of combustion-related aerosol particles, Int. J. Mass Spectrom., 258, 37–49, 2006.

Shantz, N. C., Aklilu, Y.-A., Ivanis, N., Leaitch, W. R., Brickell, P. C., Brook, J. R., Cheng, Y., Halpin, D., Li, S.-M., Tham, Y. A., Toom-Sauntry, D., Prenni, A. J., and Graham, L.: Chemical and physical observations of particulate matter at Golden Ears Provinical Park from anthropogenic and biogenic sources, Atmos. Environ., 38, 5849–5860, 2004.

Shilling, J. E., Chen, Q., King, S. M., Rosenoern, T., Kroll, J. H., Worsnop, D. R., McKinney, K. A., and Martin, S. T.: Particle mass yield in secondary organic aerosol formed by the dark ozonolysis of α-pinene, Atmos. Chem. Phys., 8, 2073–2088, 2008,
http://www.atmos-chem-phys.net/8/2073/2008/.

Shrivastava, M. K., Lane, T. E., Donahue, N. M., Pandis, S. N., and Robinson, A. L.: Effects of gas-particle partitioning and aging of primary emissions on urban and regional organic aerosol concentrations, J. Geophys. Res., 113, D18301, doi:10.1029/2007JD009735, 2008.

Singh., H., Salas, L., Herlth, D., Kolyer, R., Czech, E., Vlezee, W., Li, Q., Jacob, D. J., Blake, D., Sachse, G., Harward, C. N., Fuelberg, H., Kiley, C. M., Zhao, Y. J., and Kondo, Y.: In situ measurements of HCN and CH3CN over the Pacific Ocean: Sources, sinks, and budgets, J. Geophys. Res., 108, 8795, doi:10.1029/2002JD003006, 2003.

Slowik, J. G., Vlasenko, A., McGuire, M., Evans, G. J., and Abbatt, J. P. D.: Simultaneous factor analysis of organic particle and gas mass spectra: AMS and PTR-MS measurements at an urban site, Atmos. Chem. Phys., 10, 1969–1988, 2010,
http://www.atmos-chem-phys.net/10/1969/2010/.

Smyth, S. C., Jiang, W., Roth, H., Moran, M. D., Makar, P. A., Yang, F., Bouchet, V. S., and Landry, H.: A comparative performance evaluation of the AURAMS and CMAQ air-quality modelling systems, Atmos. Environ., 43, 1059–1070, 2009.

Spracklen, D. V., Bonn, B., and Carslaw, K. S.: Boreal Forests, Aerosols and the Impacts on Clouds and Climate, Phil. Trans. R. Soc. A., 366, 4613–4626, 2008.

Stroud, C. A., Morneau, G., Makar, P. A., Moran, M. D., Gong, W., Pabla, B., J., Z., Bouchet, V. S., Fox, D., Venkatesh, S., Wang, D., and Dann, T.: OH-reactivity of volatile organic compounds at urban and rural sites across Canada: Evaluation of air quality model predictions using speciated VOC measurements, Atmos. Environ., 42, 7746–7756, 2008.

Szidat, S., Jenk, T. M., Gäggeler, H. W., Synal, H.-A., Fisseha, R., Baltensperger, U., Kalberer, M., Samburova, V., Reimann, S., Kasper-Giebl, A., and Hajdas, I.: Radiocarbon (14C)-deduced biogenic and anthropogenic contributions to organic carbon (OC) of urban aerosols from Zürich, Switzerland, Atmos. Environ., 38, 4035–4044, 2004.

Tsimpidi, A. P., Karydis, V. A., Zavala, M., Lei, W., Molina, L., Ulbrich, I. M., Jimenez, J. L., and Pandis, S. N.: Evaluation of the volatility basis-set approach for the simulation of organic aerosol formation in the Mexico City metropolitan area, Atmos. Chem.

Phys., 10, 525–546, 2010,
http://www.atmos-chem-phys.net/10/525/2010/.

Tunved, P., Hansson, H.-C., Kerminen, V.-M., Ström, J., Dal Maso, M., Lihavainen, H., Viisanen, Y., Aalto, P. P., Komppula, M., and Kulmala, M.: High Natural Aerosol Loading over Boreal Forests, Science, 312, 261–263, 2006.

Ulbrich, I. M., Canagaratna, M. R., Zhang, Q., Worsnop, D. R., and Jimenez, J. L.: Interpretation of organic components from Positive Matrix Factorization of aerosol mass spectrometric data, Atmos. Chem. Phys., 9, 2891–2918, 2009,
http://www.atmos-chem-phys.net/9/2891/2009/.

Ulbrich, I. M., Lechner, M., and Jimenez, J. L., AMS Spectral Database. URL: http://cires.colorado.edu/jimenez-group/AMSsd/, 2009b.

Vlasenko, A., Slowik, J. G., Bottenheim, J. W., Brickell, P. C., Chang, R. Y.-W., Macdonald, A. M., Shantz, N. C., Sjostedt, S. J., Wiebe, H. A., Leaitch, W. R., and Abbatt, J. P. D.: Measurements of VOCs by proton transfer reaction mass spectrometry at a rural Ontario site: Sources and correlation to aerosol composition, J. Geophys. Res., 114, D21305, doi:10.1029/2009JD12025, 2009.

Volkamer, R., Jimenez, J. L., San Martini, F., Dzepina, K., Zhang, Q., Salcedo, D., Molina, L. T., Worsnop, D. R., and Molina, M. J.: Secondary organic aerosol formation from anthropogenic air pollution: Rapid and higher than expected, Geophys. Res. Let., 33, L17811, doi:1029/2006GL026899, 2006.

Weber, R. J., Sullivan, A. P., Peltier, R. E., Russell, A., Yan, B., Zheng, M., De Gouw, J. A., Warneke, C., Brock, C. A., Holloway, J. S., Atlas, E. L., and Edgerton, E.: A study of secondary organic aerosol formation in the anthropogenic-influenced 1 southeastern United States, J. Geophys. Res., 112, D13302, doi:10.1029/2007JD008408, 2007.

Williams, B. J., Goldstein, A. H., Millett, D. B., Holzinger, R., Kreisberg, N. M., Hering, S. V., White, A. B., Worsnop, D. R., Allan, J. D., and Jimenez, J. L.: Chemical speciation of organic aerosol during the Internation Consortium for Atmospheric Research on Transport and Transformation 2004: Results from in situ measurements, J. Geophys. Res., 112, D10S26, doi:10.1029/2006JD007601, 2007.

Xia, A. G., Michelangeli, D. V., and Makar, P. A.: Box model studies of the secondary organic aerosol formation under different HC/NOx conditions using the subset of the Master Chemical Mechanism for alpha-pinene oxidation, J. Geophys. Res., 113, D10301, doi:10.1029/2007JD008726, 2008.

Yokelson, R. J., Crounse, J. D., DeCarlo, P. F., Karl, T., Urbanski, S., Atlas, E., Campos, T., Shinozuka, Y., Kapustin, V., Clarke, A. D., Weinheimer, A., Knapp, D. J., Montzka, D. D., Holloway, J., Weibring, P., Flocke, F., Zheng, W., Toohey, D., Wennberg, P. O., Wiedinmyer, C., Mauldin, L., Fried, A., Richter, D., Walega, J., Jimenez, J. L., Adachi, K., Buseck, P. R., Hall, S. R., and Shetter, R.: Emissions from biomass burning in the Yucatan, Atmos. Chem. Phys., 9, 5785–5812, 2009,
http://www.atmos-chem-phys.net/9/5785/2009/.

Yokelson, R. J., Karl, T., Artaxo, P., Blake, D. R., Christian, T. J., Griffith, D. W. T., Guenther, A., and Hao, W. M.: The Tropical Forest and Fire Emissions Experiment: overview and airborne fire emission factor measurements, Atmos. Chem. Phys., 7, 5175–5196, 2007,
http://www.atmos-chem-phys.net/7/5175/2007/.

Yokelson, R. J., Urbanski, S. P., Atlas, E. L., Toohey, D. W., Alvarado, E. C., Crounse, J. D., Wennberg, P. O., Fisher, M. E., Wold, C. E., Campos, T. L., Adachi, K., Buseck, P. R., and Hao, W. M.: Emissions from forest fires near Mexico City, Atmos. Chem. Phys., 7, 5569–5584, 2007,
http://www.atmos-chem-phys.net/7/5569/2007/.

Zhang, J., Huff Hartz, K. E., Pandis, S. N., and Donahue, N. M.: Secondary organic aerosol formation from limonene ozonolysis: Homogeneous and heterogeneous influences as a function of NOx, J. Phys. Chem. A, 110, 11053–11063, 2006.

Zhang, Q., Alfarra, M. R., Worsnop, D. R., Allan, J. D., Coe, H., Canagaratna, M. R., and Jimenez, J. L.: Deconvolution and Quantification of Hydrocarbon-like and Oxygenated Organic Aerosols Based on Aerosol Mass Spectrometry, Environ. Sci. Technol., 39, 4938–4952, 2005.